

NOTICE: This version of the manuscript is outdated and contains several errors that were corrected in a previous version. These have been reinstated at the request of the Science Advances editorial office with the goal to “facilitate communication and exchange of information between scientists”, while the manuscript undergoes review. Most significantly, the flowchart of Figure S2 is not accurate, and several results of Text S3 are slightly misstated or have incomplete proofs.

Please contact the authors JC Rozum (jcr52@psu.edu) or R Albert (rza1@psu.edu) to discuss the scientific content.

Please contact the Science Advances editorial office (ScienceAdvancesEditorial@aaas.org) with questions regarding policies pertaining to the reinstatement of these inaccuracies. We will provide corrections as soon as the editorial office allows.

Parity and time-reversal elucidate both decision-making in empirical models and attractor scaling in critical Boolean networks

Short title: Parity and time-reversal elucidate decision-making

Jordan C. Rozum¹, Jorge Gómez Tejeda Zañudo^{2,3}, Xiao Gan^{4,5}, Réka Albert^{1,6}

¹ Department of Physics, The Pennsylvania State University, University Park, PA 16802, USA

² Eli and Edythe L. Broad Institute of MIT and Harvard, Cambridge, MA, 02142, USA

³ Department of Medical Oncology, Dana-Farber Cancer Institute, Harvard Medical School, Boston, MA, 02115, USA

⁴ Network Science Institute and Department of Physics, Northeastern University, Boston, MA 02115, USA

⁵ Channing Division of Network Medicine, Department of Medicine, Brigham and Women's Hospital, Harvard Medical School, Boston, MA 02115, USA

⁶ Department of Biology, The Pennsylvania State University, University Park, PA 16802, USA

Abstract

We present new applications of parity inversion and time-reversal to the emergence of complex behavior from simple dynamical rules in stochastic discrete models. Our new parity-based encoding of causal relationships and time-reversal construction efficiently reveal discrete analogs of stable and unstable manifolds. We demonstrate their predictive power by studying decision-making in systems biology and statistical physics models. These applications underpin a novel attractor identification algorithm implemented for Boolean networks under stochastic dynamics. Its speed enables resolving a longstanding open question of how attractor count in critical random Boolean networks scales with network size, and whether the scaling matches biological observations. Via 80-fold improvement in probed network size ($N=16,384$), we find the surprisingly low scaling exponent of 0.12 ± 0.05 -- approximately one tenth the analytical upper bound. We demonstrate a general principle: a system's relationship to its time reversal and state-space inversion constrains its repertoire of emergent behaviors.

Introduction

Many complex systems in the natural, social or technological realm exhibit emergent behavior, i.e., collective dynamics arising from the interaction of entities governed by simple rules [1–4]. Examples include phase transitions [5,6], flocking [7], consensus formation [8], and spontaneous synchronization of oscillators [9]. Modeling frameworks that are frequently used to study the collective behavior of individuals include nonlinear dynamics [10,11], agent-based models [12], cellular automata [13], and network models [14,15]. Boolean models sit at the intersection of these approaches (e.g., [16–18]). They assign a time-varying binary variable to each system entity, represented as a node in a network of interactions. They exhibit diverse long-term dynamics (attractors) that represent collective behavior (for example, consensus of individuals) and they describe the evolution toward an attractor (for example, consensus formation from an initially disordered state).

Boolean modeling of electronic circuits is well-known [19], but many other familiar models can also be viewed as Boolean models. The quenched (zero-temperature) Glauber model, a dynamic variant of the Ising model, considers the dynamics of each atom's two possible spin orientations under the influence of its neighbors [20,21]. Another example category includes models of spreading binary opinions through social networks (reviewed in [8]). The

McCulloch & Pitts neural network model introduces a propositional logic of all-or-none neuronal activation [22]; the Hopfield model also considers two activities for each neuron and assumes a complete network of interactions [23].

Boolean models are well suited to elucidate system-level decision-making, i.e., robust commitment towards one of the dynamical attractors in a multi-stable system. This has made their use especially wide-spread in biology. They were introduced by Stuart Kauffman [24] and René Thomas [25] as prototypical models for gene regulatory networks that underlie cell fate decisions (such as those that happen during cell differentiation). A large body of research has since shown that the attractors of Boolean models correspond to cell fates or stable patterns of cell activity (such as the cell cycle). Boolean models integrate and encode current knowledge of a biological process, fill any gaps of knowledge with hypothesized interactions, and predict the behavior of the system under loss-of-function, constitutive activation, or external control of system entities [25–27]. They are frequently used to study cell differentiation processes (e.g. T cell specialization [28,29]), developmental processes (e.g. patterning during embryogenesis in *Drosophila melanogaster* [30,31]), and cancer (e.g. metastatic reprogramming [32–34], prediction of targeted therapies [35,36]). Model predictions in a variety of systems were verified experimentally [34,37–41].

Alongside models of specific systems, analysis of the expected collective behaviors exhibited by generic Boolean models has also proven insightful. Ensembles of Boolean models (Random Boolean Networks) have been studied for decades (reviewed in [42–44]). These ensembles exhibit an order to chaos transition as dynamical and topological parameters are tuned. In the intermediate (critical) regime the ensembles exhibit features of biological cells, including stability against perturbations and plausible scaling laws for the number and size of attractors with the system size (see Text S1 for details). Here we answer a long-standing question about the scaling law in the presence of timing stochasticity.

Despite Boolean models' discrete nature and apparent simplicity, it is nontrivial to connect dynamical properties of decision-making to the underlying interaction network. Brute-force exploration of their state spaces is not generally feasible. A typical Boolean model of a biological process with a few dozen variables has tens of billions of states. Genome-scale models can have thousands of variables, resulting in too many states to encode in the observable universe. This challenge has motivated decades of research analyzing discrete dynamics without exhaustive state-space searches [45], for example by analyzing how feedback loops in the interaction network constrain dynamics [46,47]. While the body of research regarding how network structure constrains dynamics has proven invaluable, it is important to note that multiple Boolean systems are compatible with each interaction network. Ambiguity can be eliminated by defining a network whose graph structure unambiguously represents the update functions that govern the time evolution of each variable. One such network representation, the *expanded network* (also called the logical or prime-implicant hypergraph) [31,48–50], defines two *virtual nodes* for each entity, denoting the two possible values of its binary variable. Connections among virtual nodes encode the update functions. The structure of this auxiliary network tightly constrains the attractors of a system [33,37,51,52]. The expanded network can be used to identify control strategies that drive the system to a desired attractor [53,54]. The most parsimonious of these control strategies involve determining the so-called driver node(s) of self-sustaining circuits [55,56]. In this way, fixing the state of a few driver nodes ensures the system's convergence into a target space from any initial condition. This type of analysis has been used, for example, to pinpoint key proteins in pathological cell processes [53,55,57]. Although initially developed for Boolean models, the expanded network has been generalized to multi-level discrete and ODE analogs [57,58].

We go beyond the previous use of the expanded network and characterize each virtual node with a binary activity and impose a parity structure that facilitates the proof of new theorems about the effects of perturbations on system trajectories. With these additions, the expanded network is a complete representation of the Boolean dynamical system. In addition, we describe for the first time the time reversal of stochastically asynchronous Boolean systems. Using parity and time reversal transformations in tandem, we developed a new algorithm to efficiently identify all

attractors of large-scale Boolean systems. We apply the algorithm to answer the long-standing question of how quickly the number of attractors in asynchronous Random Boolean Networks increases with network size.

Results

We begin by recalling relevant concepts from Boolean modeling and defining the notation we use throughout. Constructing a Boolean model usually starts with the synthesis of the modeled system's interaction graph. An interaction graph is a signed directed graph whose nodes are the N entities of a system and whose edges represent positive (activating) or negative (inhibiting) influence. Each entity i is characterized by a variable X_i that can take one of two values: 1 ("active") or 0 ("inactive"). Each X_i updates its value according to the output of an *update function* $f_i: \{0,1\}^N \rightarrow \{0,1\}$ which maps every system state X to either 1 or 0. Any Boolean function can be expressed algebraically using logical operators (e.g., "not", "or", "and" with symbolic representations \neg , \vee , and \wedge , respectively). There are several schemes for determining the timing of variable updates. We use the *stochastic asynchronous update* scheme, in which at each step a single variable is randomly chosen to update its value (each variable must have a non-zero update probability; these are often chosen to be uniform). Compared with other updating schemes, this scheme removes spurious oscillations that arise from unrealistic perfect synchrony, but otherwise preserves long term behaviors [59–61]. Once the update functions are determined and an update scheme is selected, the Boolean system is fully specified. Each Boolean system induces a *state transition graph* (STG) with 2^N nodes that represent all possible system states and with directed edges from one node (system state) to another when the parent state can be updated in one time-step to attain the child state. Under stochastic asynchronous update, each node has between 0 and N outgoing edges. The *attractors* of a Boolean system are the terminal strongly connected components of the STG (i.e., they have no edges that exit the component). They are divided into two types: point attractors (also called fixed points or steady states), which contain only one state, and complex attractors, which contain more than one state. Importantly, the STG is the same for any choice of (nonzero) node update frequencies, and therefore the attractor repertoire does not depend on the precise values for the node update probabilities in the stochastic asynchronous update.

A new framework: The expanded network through the lens of parity

The *expanded network* (also called the logical or prime-implicant hypergraph) [31,48,50] was introduced as an auxiliary network constructed from the Boolean update functions. The expanded network nodes represent Boolean literals (e.g., X_i and $\neg X_i$) and its hyperedges (generalized edges that connect sets of nodes) represent prime implicants (irreducible sets of regulator states that result in $f_i(X) = 1$) of the update functions. Here we introduce a new definition of the expanded network that uses parity-related concepts and highlights its role as an invariant of the parity transformation.

The *parity transformation* acts on a Boolean system by the change of variables $X_i \mapsto \neg X_i$ for all variables X_i , mapping the original system with update functions f_i to the system governed by update functions $\neg f_i$. This mapping induces further transformations on any structure derived from the update functions, and so, in a slight abuse of notation, we say the parity transformation acts on all these structures. For example, the parity transformation relabels the nodes of the state transition graph so that all 1s become 0s and vice versa (see Figure 1). Viewing these node labels as spatial coordinates (so states lie on the vertices of a unit hypercube), the parity transformation is the spatial inversion of this hypercube through its center (see Figure 1).

Parity allows for a succinct definition of the expanded network that builds upon the eponymous structure defined in [50]. Here, we give an abbreviated discussion of this object and leave formal details to Text S2. Each node I of the expanded network, called a *virtual node*, is an ordered pair $I = (n(I), s(I))$ consisting of a system entity, in this

context denoted $n(I)$, and a value $s(I)$, which is either the constant 1 or the constant 0. There are two virtual nodes associated with each system entity i , namely $(i, 1)$ and $(i, 0)$; we call this pair of virtual nodes *contradictory*. A set of virtual nodes that does not contain any contradictory pair is called *consistent*. The activity variable for I , written σ_I , and a set of virtual nodes S is *active* (in a system state X) if all its members are active (i.e., if $\sigma_I(X) = 1$ for all $I \in S$). The activity variable σ_I updates according to the function F_I , which is governed by the usual system dynamics if $s(I) = 1$, and according to the parity transformed dynamics if $s(I) = 0$. We can therefore view the expanded network as having two layers: an “original update” layer and a “parity update” layer.

The dynamics of these activity variables are encoded in the connectivity of the expanded network. A *hyperedge* connects a set of parent virtual nodes $S = \{I_0, I_1, \dots, I_k\}$ to a target virtual node J if $\bigwedge_{I \in S} \sigma_I$ is a prime implicant of the update function for σ_J . Pictorially, we represent hyperedges with more than one parent using intermediary “composite nodes”, which correspond to “*and*” gates. For an example of a Boolean system and its expanded network, see Figure 1B,C. Hyperedges between and within parity layers encode important features of the dynamics. For example, negative influence manifests as inter-layer hyperedges. Thus, it follows from Theorem 19 of [47] that if a Boolean system lacks negative feedback loops and has no paths of opposite sign between any two nodes, then there is a change of variables that disconnects the parity layers from one another.

Arguably the most dynamically important of the expanded network’s topological structures are its *stable motifs* [50] and *stable modules* [58], which correspond to specific states of generalized positive feedback loops and determine *trap spaces* in the dynamics -- regions of the state-space that, once entered by a trajectory, cannot be exited (a system’s attractors are a notable special type of trap space). Many of our formal results rely on recasting these structures in the parity view of the expanded network as follows. A stable module M is a non-empty sourceless sub-hypergraph of the expanded network such that M does not overlap (does not share virtual nodes) with its image under parity. A stable motif is a stable module that does not contain any smaller stable module; note that this implies that a stable motif is strongly connected. Because stable modules (and thus also stable motifs) are sourceless, every virtual node in a stable module M can be maintained in its active state by other virtual nodes in M , meaning that the activity of M is self-sustaining. Once M is activated, it cannot be inactivated except via direct override of its virtual node activities by direct external controls (as opposed to inactivation via the effects of upstream pathways). Thus, M describes a control-robust trap space in which the values of certain variables are stationary [48,53]. The trap spaces corresponding to the activity of stable modules are exactly those considered by [51], with larger trap spaces (more states) corresponding to smaller stable modules (fewer constrained variables) and vice-versa. See Figure 1 for an example of the expanded network and stable motifs.

We leverage the parity properties of the expanded network to prove new results about driver node sets ([56]) and their relation to attractors. Formal statements and proofs are given in Text S3. Recall that a set of virtual nodes is called consistent if it is disjoint from its image under parity (i.e., it contains no pair of nodes of the form $(i, 1)$ and $(i, 0)$). We say that a set of mutually consistent virtual nodes S *drives* a virtual node $J \notin S$ if fixing S active yields dynamics for which all attractors have J active. We say that S drives $I \in S$ if S drives all the parents of a hyperedge targeting I (for example, any stable motif M drives all $I \in M$ and is therefore self-sustaining). Conversely, if S drives all parents of a hyperedge targeting a node that contradicts a member of S , we say that S is *self-negating*. The set of all virtual nodes driven by S is called the *domain of influence* (DOI) of S , written $DOI(S)$. This definition of the domain of influence is closely related to concepts presented in [56].

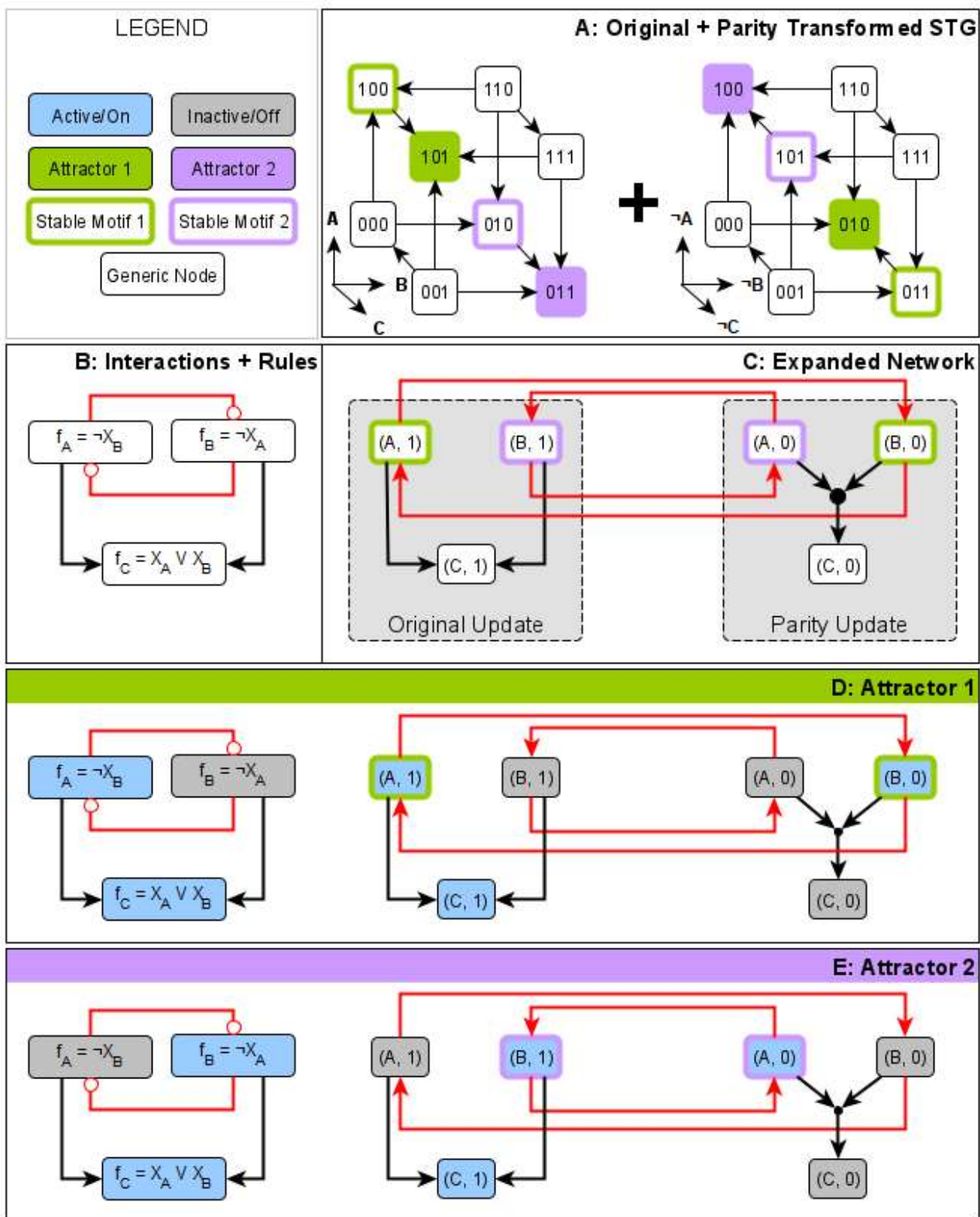


Figure 1: The relationship between the expanded network and parity transformation illustrated on a three-variable Boolean system. The state transition graphs are shown in panel A; each system state is represented as the triple $X_A X_B X_C$. Each state with fewer than three outgoing edges (state transitions) also has a self-loop, which is omitted for visual clarity. The interaction network and update functions are indicated in panel B and the expanded network in panel C. The system has two attractors, shown in panels D and E, with blue nodes active and grey nodes inactive. These two attractors (D and E) are indicated in green and purple, respectively. States in the state transition graphs of panel A are arranged so that the individual variables define coordinate axes. In this arrangement, the states form the corners of a cube. The parity transformation reflects each attractor through the center of this cube. The expanded network in panel C has two parts, or layers: regular virtual nodes (A,1), (B,1) and (C,1), whose activity updates according to the usual update functions, and negated virtual nodes (A,0), (B,0) and (C,0) that use the parity transformed update functions. The filled black circle represents the hyperedge from the set $\{(A,0), (B,0)\}$ to $(C,0)$ and indicates the “*and*” operation in the update function of the virtual node $(C,0)$. Positive regulation (black arrows) stays within a layer of the expanded network, while negative regulation (red arrows) crosses between layers. Virtual nodes (A,1) and (B,0) form a stable motif (green outline), as do the virtual nodes (A,0) and (B,1) (purple outline). In any state of the system, half of the expanded network is active. For example, attractor 1 (panel D) has the virtual nodes $(A,1), (C,1), (B,0)$ active (indicated in blue). The stable motif $\{(A,1), (B,0)\}$ describes the trap space containing Attractor 1 and does not overlap with its parity transformed set $\{(A,0), (B,1)\}$, which corresponds to the trap space containing Attractor 2 (panel E).

Calculating $DOI(S)$ can be difficult in general, so we focus instead on a commonly used and easily calculated subset of the driving relation: the logical domain of influence (LDOI). A set S of virtual nodes *logically drives* a virtual node I (which may or may not be in S) if there is a path in the expanded network hypergraph from a subset of S to I with all virtual nodes in the path consistent with S (this requires that I is consistent with S). The set of all I logically driven by S is called the *logical domain of influence* of S , written $LDOI(S)$ (or $LDOI(i, s)$ when $S = \{(i, s)\}$ is of size one). Intuitively, $LDOI(S)$ corresponds to the variable values that become fixed after percolating S through the update functions and simplifying algebraically. As demonstrated in [56], if S is a subset of $LDOI(S)$, then $LDOI(S)$ contains a stable motif. If $LDOI(S)$ contains a stable motif M , we say that S (logically) drives M .

Our main result in this section states that if S is active in some part of an attractor, then $DOI(S)$ is also active somewhere in that same part (Theorem 1, Text S3). This result illustrates how the domain of influence of a set of virtual nodes can constrain which states must coexist within an attractor. Such considerations are important in constructing Boolean models in which certain system configurations should correspond to different long-term qualitative system behaviors (e.g., phenotypes). Two corollaries of this result allow one to study the conditions under which an attractor avoids activating a particular set of stable motifs. This problem is of interest, for example, in biology, where one or more stable motifs may correspond to a diseased state of the system; the goal in this case is to identify drug targets that avoid stabilizing the diseased state. We will also make use of these results in later sections to enumerate a system’s attractors.

The first of the two corollaries (Corollary 1, Text S3) can be viewed as a compatibility condition for a stable motif’s activity and the activity of a virtual node that drives it. In the context of system control, it states that if fixing X_i is sufficient to eventually activate a stable motif M , then the oscillation of X_i is also sufficient to activate M . It can also be viewed as a consistency condition for attractors: if $X_i = s$ leads to activation of M , then we cannot have $X_i = s$ in an attractor (even transiently) in which M is inactive. This result provides a powerful way to identify circumstances in which no stable motif activates: in such cases, all stable motif drivers must be permanently inactive. Specifically, we collect all single-node drivers of all stable motifs into a set Δ , and test whether or not $\neg\Delta = \{(i, \neg s) : (i, s) \in \Delta\}$ is self-negating. If it is self-negating, then it follows that at least one element of $\neg\Delta$ is not permanently active in each attractor, and thus (by Corollary 1) this element must eventually stabilize at least one stable motif. The formal statement of this result is given as Corollary 2 in Text S3.

Time-reversal of Boolean systems and stable motifs of the time-reversed system as unstable “Gardens of Eden”

A second set of foundational results we introduce in this work is the construction of the time reversal of an asynchronous-update Boolean system -- despite the system's inherent stochasticity. We use the time reversal transformation to help identify discrete analogs of unstable manifolds in the state space. The *time reversal* of a Boolean system governed by update functions f_i is called the time reversed system and is governed by the update functions f_i^- , where $f_i^- = \neg f_i(X_i = \neg X_i)$. Like the parity transformation, we formally define the time reversal as a transformation of the Boolean system given by its effect on the update functions. It similarly induces transformations of structures that are derived from these functions. For example, the state transition graph of a system is related to its time reversed counterpart by reversing the direction of all edges (see Figure 2A). Thus, one may follow the evolution of the time reversed system on the STG by following edges in the reverse direction. Equivalently, and in analogy to concepts in solid-state physics, one may imagine that all but one of the nodes in the STG are occupied by walkers who may not share an STG node. If the walkers randomly follow the edges of the STG, then the position of the unoccupied “hole” evolves according to the possible trajectories of the time reversed system.

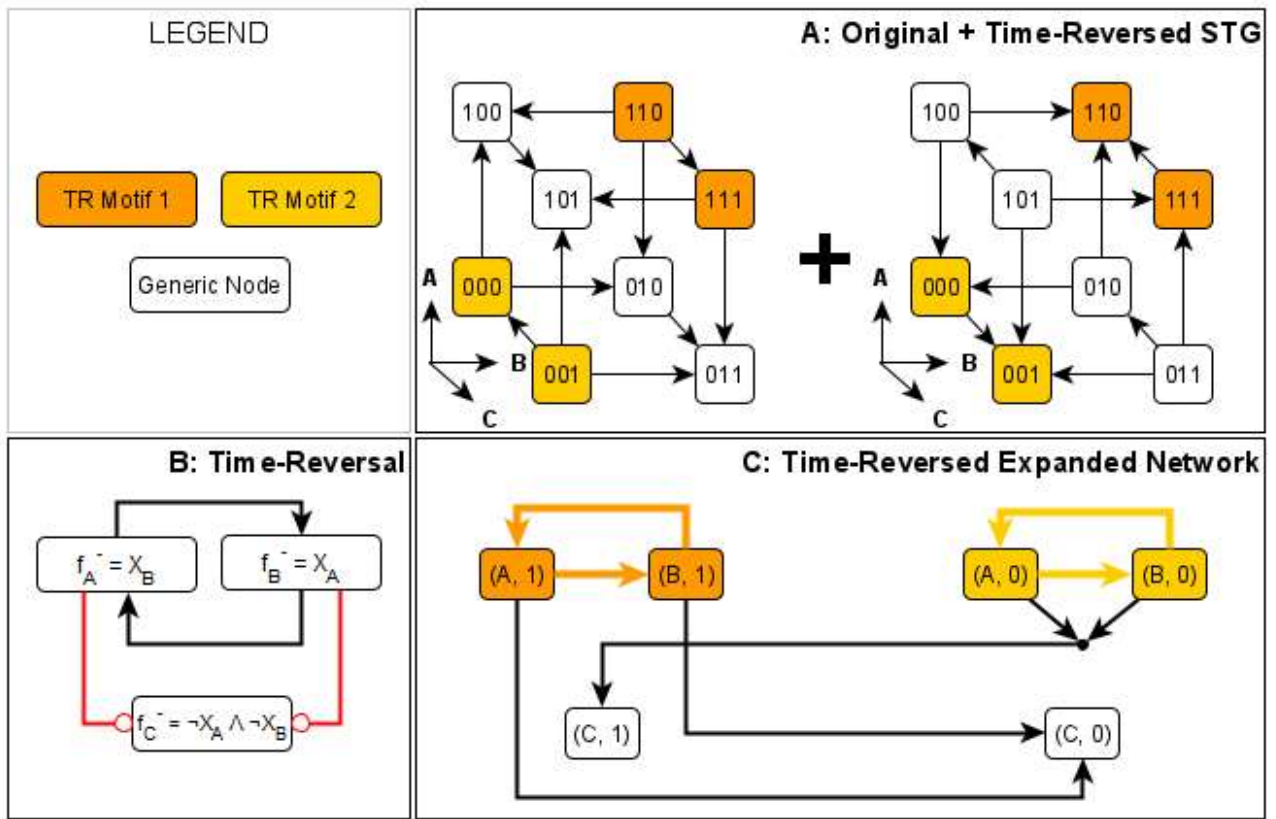


Figure 2: Illustration of the time reversal transformation on the example from Figure 1. Panel A shows the original system's STG alongside the STG of its time reversal. The time reversal has the effect of reversing the direction of each edge in the STG. The interaction network and update functions of the time-reversed system are depicted in panel B alongside its expanded network in panel C. Red interaction network edges indicate inhibition, while black edges indicate activation. The virtual nodes and hyperedges of the time-reversed system's two stable motifs are highlighted in yellow and orange in the expanded network, and the regions of state space in which they are

active are highlighted in the system's STG on the left in panel A. Note that the system states highlighted in yellow (000 and 001) viewed in the original system's STG form a subgraph that has no in-component and the state 001 is a Garden of Eden state. The same is true for the system states highlighted in orange. In this example, the sign of the regulation (inhibition vs activation) is reversed under the time reversal. This holds in general for all interactions except self-regulation, which does not change sign under time reversal.

The concept of Garden of Eden states, which are source nodes of the STG [62,63], can be generalized as subgraphs of the STG that do not have incoming edges; we call these subgraphs Garden of Eden spaces. They are analogous to unstable manifolds of ODE systems in the sense that no trajectory can enter these spaces from the outside. Any trap space of a system, and in particular any of its stable motifs, is a Garden of Eden space in the time reversed system, and vice versa. For example, the states marked in green in Figure 1A form a trap space of the original system and a Garden of Eden space of its time-reversed counterpart while the states marked in yellow form a trap space of the time-reversed system and a Garden of Eden space of the original system. An important consequence of this time reversal-based mapping between trap spaces and Garden of Eden spaces is that no attractor of a system can cross the boundary of any of the system's trap spaces or Garden of Eden spaces. This observation is especially helpful in eliminating states from consideration when searching for attractors via direct STG construction, or in reducing the number of relevant initial conditions for study. We leverage these methods to construct an efficient attractor-identification algorithm and explore their utility by way of example in the section "Application to decision-making in empirical biological network models".

Stable motif succession determines state-space decision-making and attractors

As a Boolean system's state transition graph (STG) has 2^N nodes and up to $2^N N$ edges (for stochastic asynchronous update), for systems with many entities (large N) it is impractical to use the state transition graph to determine the system's attractor repertoire. Stable motif, or trap space, based attractor identification methods are often more effective [48,50]. In the iterative approach of [50], a system's stable motifs are identified, and one is selected to "lock in". The system is then reduced under the assumption that the system's state is confined to the region described by the stable motif, resulting in a *reduced network*. Rephrased in our framework, each stable motif is selected in turn and the expanded network is simplified under the assumption that the motif's virtual nodes are active, resulting in a reduced Boolean system. We use the notation $Red(f, M)$ for the reduced system that results from a Boolean system with update function f after assuming that stable motif M is active. The process is repeated for each reduced system until all possible permutations of stable motif activation are explored. The result is a *succession diagram*, Σ , which is a directed acyclic graph whose nodes are the unions of stable motifs used to obtain each reduced system (see Text S2 for a formal definition). For an example of this process and the resulting succession diagram, see Figure 3.

The succession diagram serves as a summary of the decisions in the system dynamics that lead to successively more restrictive nested trap spaces. Each node of the succession diagram corresponds to a region of the state space in which the denoted stable motifs are active. Each branch point in the succession diagram represents potential choices to be made; which choice is ultimately selected by the system depends on various factors including the stochastic update order. It follows from the nestedness of these trap spaces that the system cannot transition between regions that are not connected by a path in the succession diagram, i.e., the succession diagram encompasses the entire repertoire of decisions the system is capable of making. The close relationship between the succession diagram and branch points in the dynamics is illustrated in Figure S1 by constructing the full state transition graph of the example from Figure 3. In the section "Application to decision-making in empirical biological

network models" below, we illustrate how the succession diagram can be used to analyze the complex state space decision-making in systems biology models.

One must take special care to consider the possibility of oscillations that avoid activation of stable motifs. For example, consider the system shown in Figure 4

$$f_A(X) = f_B(X) = \neg X_A \wedge \neg X_B \vee X_C; f_C(X) = X_A \wedge X_B.$$

This system contains only one stable motif, $\{(A, 1), (B, 1), (C, 1)\}$, which corresponds to the system's sole point attractor $X_A = X_B = X_C = 1$. Previous stable motif or trap-space based methods [50,51] would correctly identify this point attractor by finding the corresponding stable motif. This system, however, contains an additional attractor in stochastic asynchronous update. In the second attractor, X_C remains in the 0 state, while X_A and X_B oscillate; this second attractor is not identified by previous iterative stable motif reduction methods. For a detailed discussion of the nature of these oscillations and their implications for the completeness of the attractor repertoire identified by iterative stable motif reduction, see [53]. Such oscillations motivate us to propose more robust automated methods that can identify oscillations that fail to activate stable motifs. These methods make practical what previously was impractical: the identification of the attractor repertoire of ensembles of large Boolean systems. Importantly, our method automatically identifies all complex attractors, including those that were overlooked by previous iterative stable motif reduction methods.

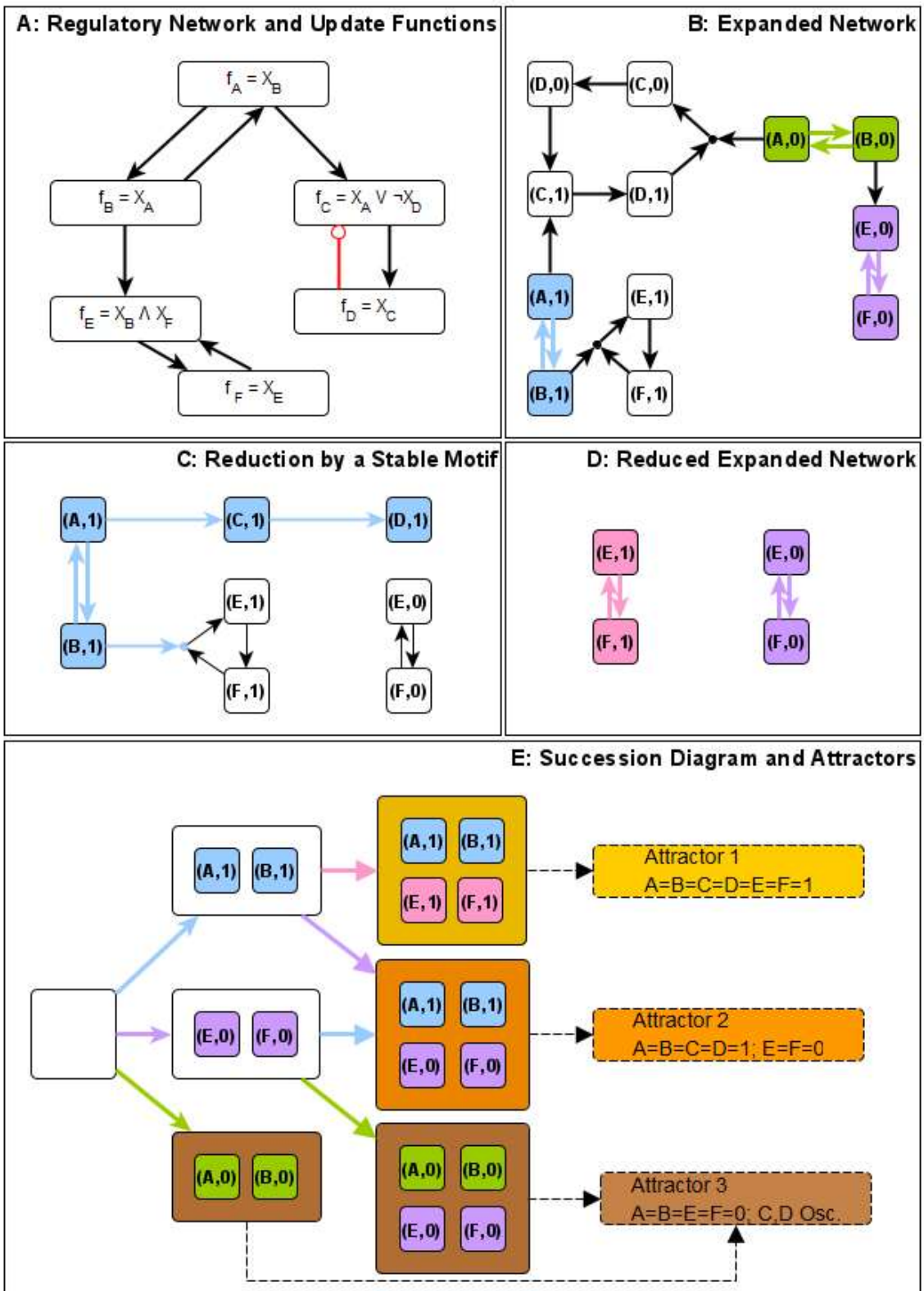


Figure 3: Outline of the iterative stable motif reduction process on a simple example. Panel A depicts a Boolean system's interaction network and update functions. The corresponding expanded network is shown in panel B; there are three stable motifs, highlighted in blue, green or purple. In panel C, the stable motif corresponding to $X_A = X_B = 1$ is selected and the effect of maintaining its activity is highlighted in blue; in particular, it leads to $X_C = X_D = 1$. The variables that are unfixed (X_E and X_F) then form a bistable system whose expanded network is shown in panel D. The reduced system has two stable motifs, highlighted in pink or purple; the latter was also a stable motif of the original system. All possible sequences of stable motif selection and reduction are summarized in a succession diagram (panel E). Each node of the succession diagram is a set of virtual nodes that contains the stable motifs that were selected for use in the reduction. The colors of the edges in the succession diagram indicate which stable motif is selected to get from one reduction to the next. The process terminates when no stable motifs remain, and the attractors of the maximally reduced systems are identified as attractors of the unreduced system (highlighted in yellow, orange, and brown).

Overview of the attractor identification algorithm

We follow an iterative stable motif approach to attractor identification in which stable motifs are recursively used to produce reduced Boolean systems (and corresponding reduced logical hypergraphs) until no additional stable motifs remain (see Figure 3). At each stage in the iteration, we identify whether the reduced system permits any complex attractors that do not activate any additional stable motifs. We call such attractors *motif-avoidant* and call reduced systems with motif-avoidant attractors *terminal*. Though terminality requires analysis of the system's state transition graph in the general case, it is usually possible to significantly reduce the computational burden by application of a necessary condition for terminality that arises from Corollary 2 (Text S3) and properties of the parity expanded network. We derive this condition in Text S4, where we consider the set Δ of all virtual nodes that individually drive any stable motif to obtain the following result: all motif-avoidant attractor states satisfy $R(X) = 1$, where $R(X) = \bigwedge_{I \in \neg \Delta} (\sigma_I(X) \wedge F_I(X) \wedge (\bigwedge_{J \in LDOI(I)} \sigma_J(X)))$ (and $R(X) \equiv 1$ when Δ is empty). This result is a necessary consistency condition for the inactivity of stable motif drivers. In the example of Figure 4, there is only one single-node driver of the system's sole stable motif, namely $(C, 1)$. Thus, the entire negated driver set is $\neg \Delta = \{(C, 0)\}$. We calculate that $LDOI(C, 0)$ is empty and that the update function for $(C, 0)$ is $F_{(C, 0)} = \neg X_A \vee \neg X_B$. Therefore, we find $R(X) = \neg X_C \wedge (\neg X_A \vee \neg X_B)$. In panel C of Figure 4, only the three yellow states have $R(X) = 1$, and so any motif-avoidant attractor is confined to those three states.

We also leverage time reversal in determining terminality. If a stable motif M^- of the time-reversal of G is active in a state X , then X can only be in an attractor of G if M^- (viewed as a set of virtual nodes in the forward-time system) is not self-negating in G . Thus, when considering states that may be in a motif-avoidant attractor of G , we can ignore states belonging to stable motifs of G , belonging to self-negating stable motifs of $TR(G)$, and states for which $R(X)$ is zero. We call the remaining states the *terminal restriction space* of G . For example, the terminal restriction space of the system in Figure 4 is the yellow portion of its state transition graph. In practice, focusing on the terminal restriction space can reduce the number of variables that must be simulated by a considerable amount. For example, we analyzed the 60-node T-LGL network of [64], whose STG is too large (hundreds of petabytes or more) to practically construct. Previous stable motif-based algorithms can estimate the attractor repertoire in a matter of hours, but cannot guarantee the absence of motif-avoidant attractors without building the STG [50]. Exploring only the terminal restriction space, however, results in a reduction of the search-space by a factor of over two billion and allows us to exactly identify all the attractors of the system in a matter of minutes. (For the purposes of making explicit comparisons to a fully constructed STG, we analyze a simplified model of this same system, due to [65], in Text S6). We have also found many examples of random Boolean networks ($K = 2, p = 0.5, N = 4096$) in which the terminal restriction space of the initial network is of size zero; a state-space reduction of 2^{4096} . For a description of

the algorithm we use to efficiently search the reduced terminal restriction state space for motif-avoidant attractors, see Text S5.

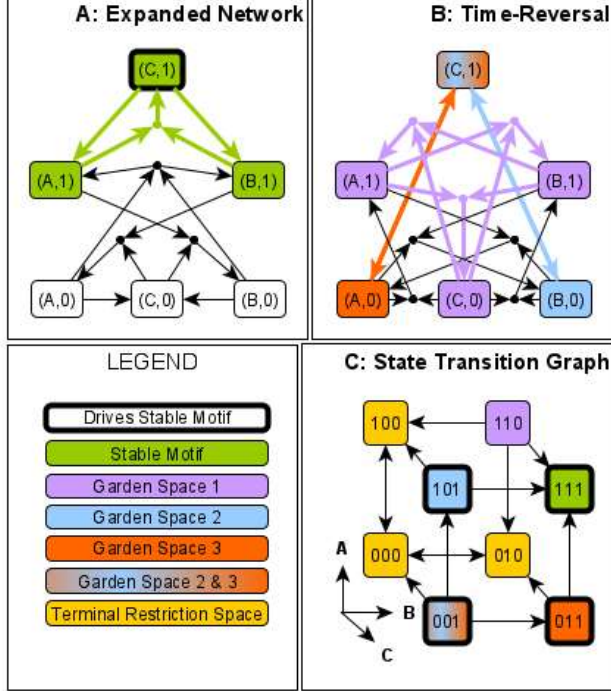


Figure 4: An illustration of methods to refine the portion of the STG that may contain stable motif-avoidant attractors using the system $f_A(X) = f_B(X) = \neg X_A \wedge \neg X_B \vee X_C$; $f_C(X) = X_A \wedge X_B$ as an example. Panel A presents the system's expanded network and its sole stable motif (in green). This stable motif has one driver set, $\{(C,1)\}$ (bold outline). By Corollaries 1 and 2 (Text S3), any motif-avoidant attractor must have $X_C = 0$ and $F_{(C,0)} = \neg X_A \vee \neg X_B = 1$ fixed, i.e., such an attractor can only contain states that satisfy $R(X) = \neg X_C \wedge (\neg X_A \vee \neg X_B) = 1$. Panel B shows the expanded network of the time-reversed system, with its three stable motifs highlighted in purple, blue, and orange. Panel C shows the STG of the system. The states corresponding to each of the stable motifs in panels A and B are highlighted in matching colors. States with $(C,1)$ active are highlighted with a bold outline; none of these states can be part of a stable motif-avoidant attractor. The three stable motifs of the time reversal partition the STG into five subgraphs based on which time reversal stable motifs are active: none, purple, blue only, orange only, or both orange and blue. These subgraphs, highlighted by color, are Garden of Eden spaces of the forward-time system. No attractor of the forward-time system can cross between these regions. Any motif-avoidant attractor of the system must reside in the terminal restriction space of the STG (yellow). Indeed, the states 100, 000, and 010 form a motif-avoidant attractor in which $X_C = 0$ is fixed while X_A and X_B oscillate.

In some cases, even the terminal restriction space is too large to simulate. In these cases, we can obtain information about the number of motif-avoidant attractors via the network reduction method of [66,67]. Variables that do not self-regulate are iteratively “deleted” by substituting their update functions into their successors’ update functions (see Figure 5). This method, which we call *deletion projection*, provides a projection map, π , that is proven to preserve both point attractors and complex attractors. The inverse map preserves all point attractors, but only a subset of complex attractors in general (in other words, the projected system can have additional “spurious” complex attractors). We combine the concepts of stable motifs and driver nodes with the deletion projection method of [66,67] to investigate the terminality of a motif-reduced Boolean system. We show that the domain of influence of a set of

virtual nodes that specifies a state for every variable in the projected system has a domain of influence in the unprojected system that specifies exactly one state, called a “representative state” in [91] (Lemma 1, Text S3). Combining this result with Theorem 1 (Text S3) leads to one of our main results of this section: the activity of stable motifs in attractors is preserved by the deletion projection (Theorem 2, Text S3). Theorem 2 allows us to test the terminality of a system by testing the terminality of its projection.

We give a visual overview of the algorithm in Figure S2. We also present a “by hand” example of the approach on a five-variable system in Figure S3. We implement the techniques described in this section in the `StableMotifs` Python Library (available at <https://github.com/jcrozum/StableMotifs>). Notably, our attractor-finding method outperforms the earlier stable motif-based method of [50]. For example, our code was able to compute the succession diagram of the 69-node unstimulated epithelial-to-mesenchymal transition model of [33] in under two minutes on a consumer-grade laptop, while the software implementation of [50] was unable to do so within twenty-four hours.

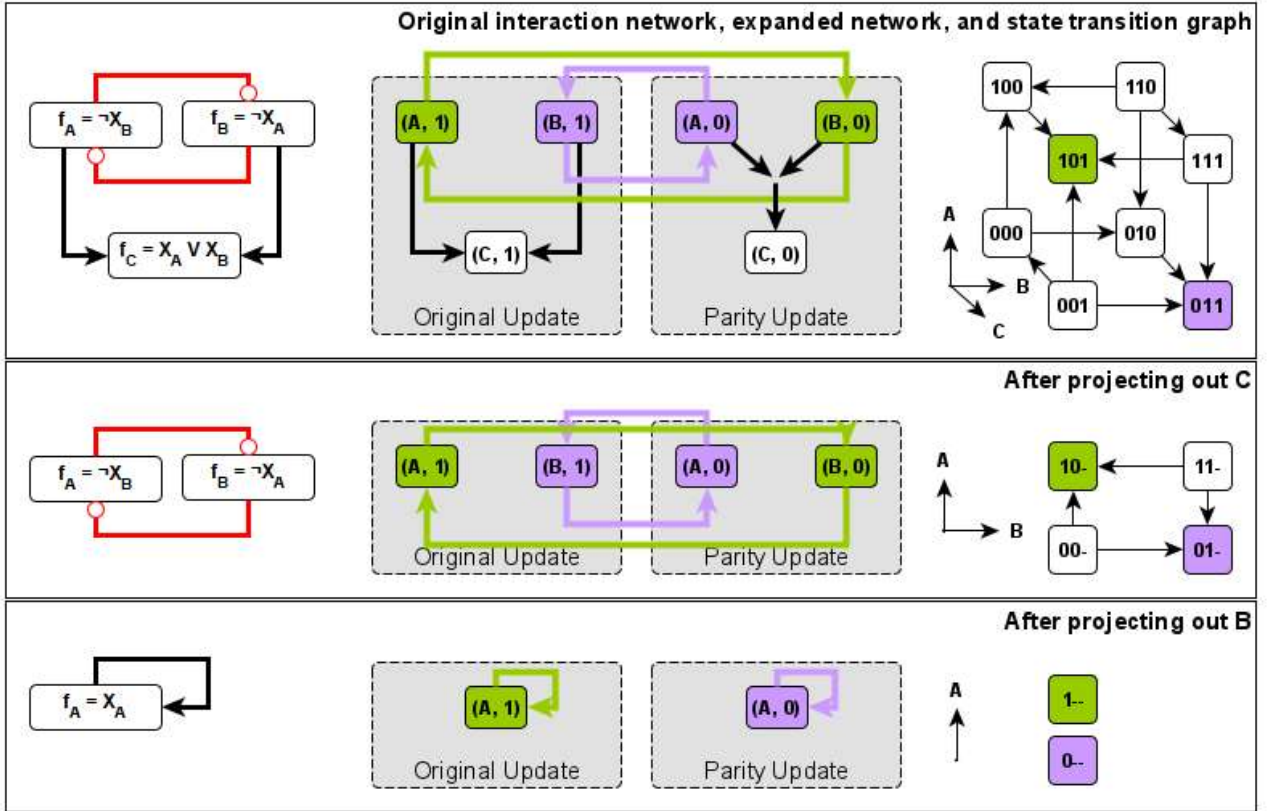


Figure 5: Deletion projection example. Each panel shows the interaction network, expanded network, and STG of a system before projection (top), after projecting out one variable (middle), and after projecting out two variables (bottom). The attractors of each system and the stable motifs that are active therein are highlighted in green and purple. Attractors and stable motifs project onto attractors of the same color. The projection procedure preserves point attractors exactly. In general, the number of complex attractors (in this case zero) serves as an upper bound on the number of complex attractors in the unprojected system (see, e.g., [66]). One may view the action of the projection on the STG as contracting the top four nodes (100 , 101 , 110 , and 111) to a single node ($1--$), with representative state 101 (transitions among these four nodes ultimately lead to 101); a similar view can be taken of the bottom four nodes. We note that the projection procedure respects the parity layer partitioning of virtual nodes. In accordance with Theorem 2, the stable motifs $\{(A, 1), (B, 0)\}$ and $\{(A, 0), (B, 1)\}$, which project to the self-

activating virtual nodes $(A,1)$ and $(A,0)$, respectively) are preserved in the sense that, for example, the attractor with $(A,1)$ active in the bottom panel corresponds to an attractor in which the stable motif $\{(A,1),(B,0)\}$ (which projects onto $(A,1)$) is active. This implies that the value of X_A is sufficient to determine which attractor the system attains.

Application to decision-making in empirical biological network models

In this section we illustrate how our methods can be applied to validated Boolean models of biological networks to analytically connect regions of state space to decision-making (points-of-no-return) in their dynamics and to subnetworks (stable motifs) in the underlying interaction network. The biological network models we focus on are a model of the mammalian cell cycle Phase Switch [68] (presented in the subsection below) and a model [65] of a type of white blood cell cancer (T-LGL leukemia) (presented in Text S6). In particular, we identify and characterize the Garden of Eden spaces, illustrate an informative partitioning of the state space, and fully describe the attractor basins.

Decision-making in the cell-cycle network dynamics

The Phase Switch is a tri-stable molecular circuit that drives mitosis. Its three steady states mark three stages of the cell cycle: G1, G2, and the spindle assembly checkpoint (SAC). Under various biologically relevant conditions, such as coupling to other molecular circuits, the Phase Switch oscillates between these stages in the order they occur in the cell cycle [52] -- here, however, we study this switch in isolation. Further details of this model, including the update functions and stable motifs, are given in Text S7.

Our focus is on how details of a system's decision-making capacity can be explored by analyzing the system's time reversal in conjunction with the succession diagram. We emphasize insights gained from the stable motifs of the time-reversed system. In principle, more granular initial condition tracing is possible via the full succession diagram of the time-reversed system. Figure 6 shows how the succession diagram and Garden of Eden spaces provide a concise summary of the irreversible commitments in state space; this is especially useful when the state transition graph is too large or too dense to analyze directly (compare panels B and E). The compressed state space illustration of Panel E unites information from the original and time-reversed system. It is equally or more informative than the full state transition graph (panel B). The compressed succession-diagram representation has the benefit that it can be constructed for very large networks whose state transition graph cannot be built. Indeed, as we will demonstrate in the next section, we can build succession diagrams for networks whose state transition graphs have more nodes ($\approx 2^{4000}$) than can physically exist in the observable universe ($\approx 2^{600}$, assuming one state per Planck volume and disregarding graph edges).

An important feature of this analysis is that decisions can be ascribed to specific strongly connected subgraphs of the interaction network. These subgraphs and their stable states correspond exactly to stable motifs, i.e., their representations in the parity-expanded network do not have any parity-invariant subgraphs. These can provide important biological insights. For example, because there are no paths in the succession diagram from P1 to SAC (Figure 6C), we see that the P1 stable motif cannot be active during the spindle assembly checkpoint (SAC) phase. Driver node analysis of the Cdk1-Wee1 feedback associated to the P1 stable motif (Figure 6D) indicates that knockout of Cdk1 alone blocks the spindle assembly checkpoint. Following P1 commitment, the choice between G1 and G2 is decided by the activity of the Cdc25A-CyclinA feedback loop (P0) in competition with the Cdh1-CyclinA feedback loop (P6) when pAPC is inactive (P5).

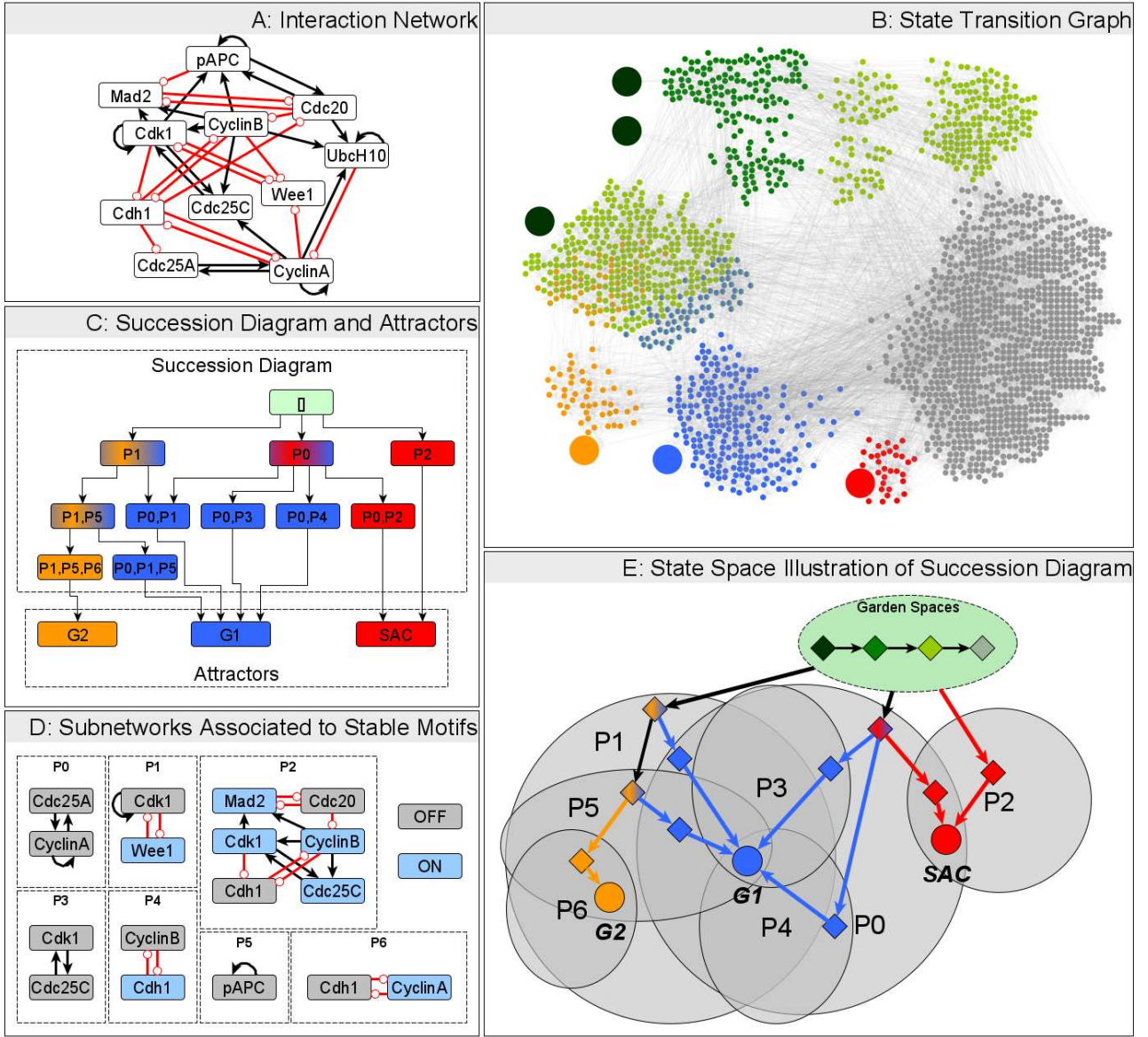


Figure 6: Parity and time-reversal analysis elucidates state-space decision-making in the Phase Switch model of [68]. Text S7 provides further details about the model, including its update functions. The interaction network is presented in panel A. The full state transition graph is indicated in panel B. The three point attractors of this model are the three large nodes highlighted in blue, yellow, and red, and correspond to the G1, G2, and SAC phases of the cell cycle. The basins of attraction exclusive to each attractor are highlighted in the matching color. Grey nodes have paths to multiple attractors; the path taken depends upon the stochastic update order. The stable motifs of the time reversed system identify unstable “Garden of Eden” regions of the state space (highlighted in green) which cannot be (re)entered from the outside. A darker shade of green indicates the overlap of multiple Garden of Eden spaces. The three large green nodes are the “Garden of Eden” states of the system, and are obtained analytically as the fixed points of the time-reversed system. Panel C shows the stable motif succession diagram of the system, with stable motifs of the network and reduced network denoted by labels P0-P6. The colors indicate, by the same scheme as in panel B, which attractors are possible after commitment to each stable motif. Panel D shows the subnetworks and node states associated with these stable motifs (blue: active/on, grey: inactive/off). These subnetworks and their states are obtained as strongly connected components of the expanded network that do not contain parity-invariant subgraphs. In panel E, we illustrate how the succession

diagram and garden spaces together describe (analytically) the possible decisions the system can make during its dynamics. Ovals represent specific subsets of the state space. The green oval stands for “Garden of Eden” spaces, with the internal diamonds representing generic states in several categories of these spaces: the darkest green diamond represents Garden of Eden states (fixed points of the time reversed system); the green diamond represents states in the overlap of multiple stable motifs in the time reversed system; the light green diamond represents states in a single stable motif of the time reversed system; and finally, the grey diamond represents states that do not lie in any stable motif of either the forward or backward time system. That states of this last type belong in a Garden of Eden space follows from the definition of stable motifs and the lack of motif-avoidant attractors in this system. Progression from darker to lighter green represents the commitment to exiting Garden of Eden spaces. Grey ovals represent overlapping spaces determined by the stable motif written inside each oval. The diamond symbols in these overlaps mark relevant trap spaces, e.g. the yellow diamond marks the trap space in which motifs P1, P5 and P6 are all active. Each edge corresponds to an irreversible commitment to a smaller trap space. For example, the yellow-blue diamond marking the intersection of the P1 and P5 spaces has two edges: the edge to the yellow diamond indicates a transition to the intersection of the P1, P5 and P6 motif regions, which determines an irreversible commitment to G2 (entry into the exclusive basin of attraction to G2), and the edge to the blue diamond indicates a transition to the intersection of the P0, P1 and P5 motif regions, which determines an irreversible commitment to G1 (entry into the exclusive basin of attraction to G1). Circular symbols indicate the attractors and highlight their position in the narrowest trap space. The graph structure in panel E is isomorphic to the graph structure in panel C, demonstrating that the stable motif succession diagram encapsulates the trajectory of the system in state space.

Random Boolean network results

As an additional application we study the scaling of the average number of attractors of ensembles of RBNs generated by the Kauffman $N - K$ model [24]. In this model, each of N nodes receives K edges from randomly selected “regulator” nodes. Each node’s (quenched) update function randomly maps each of the 2^K possible combined regulator states to 1 with probability p or to 0 with probability $1 - p$. Tuning the indegree K or the activation bias p yields an order-to-chaos transition at $2Kp(1 - p) = 1$ (in the thermodynamic limit, when $N \rightarrow \infty$) [42,69–71]. For additional details about previous studies of this model, see Text S1. We address and resolve the open problem of the attractor number scaling in the critical $K = 2$, $p = 0.5$ regime under stochastic asynchronous update. The number of attractors provably scales as a power law asymptotically bounded above by N^{1/n_4} [72]. In this section, we obtain the current best numerical estimate of the scaling exponent value (see Supplementary Code and the Random Boolean Network Application folder at <https://github.com/jcrozum/StableMotifs/> for details on ensemble generation and analysis).

We generate ensembles for increasing network size N (from size $N = 2$ to size $N = 4,096$) and apply our attractor identification algorithm to construct the succession diagram for each network and to determine or bound (in networks that are unusually computationally difficult) its number of attractors. For greater than 96% of the more than 10,000 unique networks generated we are able to exactly enumerate the attractors, and this fraction never falls below 86% (260/300 for $N = 2,048$) for any value of N considered here. For all but 13 (0.1% of the total) of the networks without an exact attractor count we can constrain the number of attractors by using the deletion projection and/or counting the number of maximal stable modules (see Supplementary Code for details and implementation). Of these thirteen networks, the plurality (5) are of size 4,096, corresponding to 1.67% of the 300 networks generated for this size. For each of these remaining thirteen, we use the trivial lower bound of 1 for the number of attractors and choose an upper bound 10% larger than that of the most attractor-rich networks of the same size (see Supplementary Code for details). This makes these networks outliers without introducing undue sensitivity.

The scaling of the average number of attractors $\langle A \rangle$ as a function of network size N is shown in Figure 7.

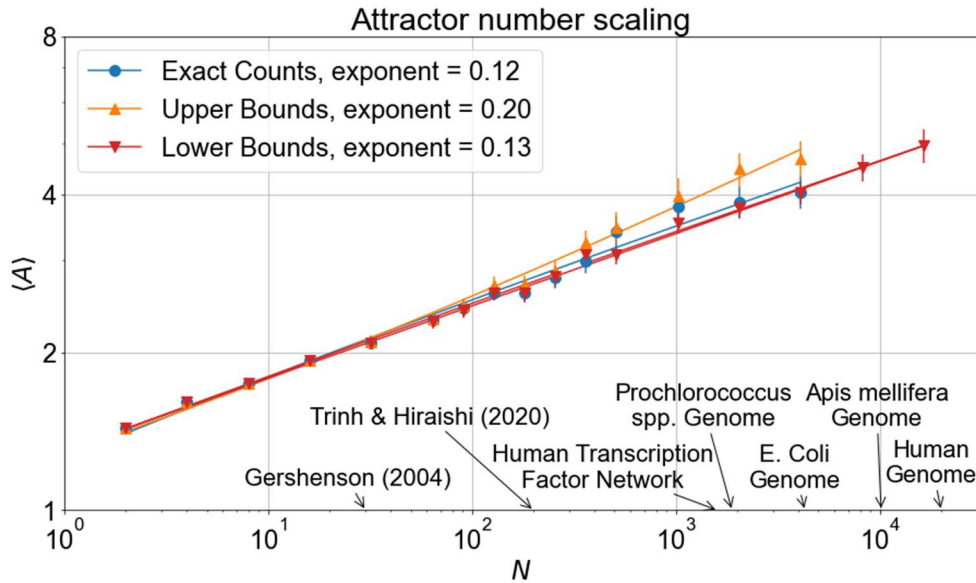


Figure 7: Summary of RBN attractor scaling fits. Symbols indicate the measured number of attractors and the lines represent fits of the form $\langle A \rangle = a + bN^c$ using nonlinear least-square fitting (see Supplementary Code for implementation details). The fits yield intercept $a = -0.38$, $a = 0.44$, and $a = -0.16$ for the exact counts, upper bounds, and lower bounds, respectively. The exponents of the fits (c in $\langle A \rangle = a + bN^c$) are reported in the legend; see the main text or Supplementary Code for bootstrapped confidence intervals. For reference, the sizes of previously considered asynchronous RBN ensembles ([73,74]) and several genetic networks from biology [75–79] are annotated on the horizontal axis.

By fitting power law $\langle A \rangle = a + bN^c$ we find that the exponent is $c = 0.12 \pm 0.05$ (one standard deviation; 95%CI [0.04,0.22]) when fitting only the networks for which we are able to exactly enumerate the attractors (blue circles and curve on Figure 7). The attractor upper bounds (orange symbols and curve) yield an upper bound on the scaling exponent of $c = 0.20 \pm 0.05$ (95%CI [0.11,0.30]). To ensure that the considered networks are sufficiently large, we analyze the scaling of the number of maximal stable modules in networks as large as $N = 16,384$ (recall that stable modules are source-free subgraphs of the expanded network that have no parity-invariant subgraphs). Because maximal stable modules correspond to disjoint trap spaces in the state space, their number serves as a lower bound on the number of attractors. We include these lower bounds in our analysis of the lower bound scaling. In practice, the lower bounds are very often in 1-1 correspondence with the number of attractors, as is supported by the good agreement between the exact count of attractors and the lower bounds on the attractor counts. In particular, the scaling of the lower bounds ($c = 0.13 \pm 0.04$, 95%CI [0.06,0.21]) is consistent with the attractor scaling for $N \leq 4096$ and continues at least until $N = 16,384$, providing strong support that we have probed sufficiently large networks. These networks are of comparable size to many frequently studied genomes (e.g., $N \approx 4,000$ for the *E. coli* genome, while for the Human genome, $N \approx 20,000$). All the scaling exponents are well below the initially conjectured square root scaling ($c = 0.5$) and the theoretical maximum of $c = \ln 4 (\approx 1.39)$. For additional details regarding the fitting procedure and error estimation, see Supplementary Code.

Overall, we obtain the best current estimate of the exponent of $K = 2, p = 0.5$ Kauffman networks under stochastic update. Our analysis represents an 80-fold increase in network size over previous exact or near-exact enumeration analysis of asynchronous $N - K$ RBNs [73,74]. We find a significantly lower exponent than the original exponent found by Kauffman and those identified in other stochastic updating schemes [72-74].

Discussion

Two central questions in complexity science are “what emergent behaviors could a complex system exhibit?” and “what controls a complex system’s selection of one emergent behavior or another?”. While interesting questions from a purely theoretical perspective, they also have important applications in engineering, social science, and medicine. The past several decades have seen a growing number of collaborations between biologists, computer scientists, mathematicians, and physicists that approach these questions using Boolean networks. This work continues that interdisciplinary tradition, using geometric intuitions from physics to prove new results in the mathematics of Boolean dynamics, which we have applied to develop improved computational methods for analyzing complex systems common in biology and other sciences. Coming full circle, these methods have yielded new results in the statistical mechanics of random Boolean networks. Our methods allow efficient identification of the subspaces of the state space where robust commitments happen, and connect these decision-making spaces to subnetworks in the underlying interaction network. Time reversal identifies a previously unexplored type of decision-making: the commitment to exit a “Garden of Eden” space, eliminating the option to ever return to that space. We associate each decision with the stabilization or de-stabilization of strongly connected subnetworks that do not contain any parity-invariant parts.

The parity symmetry of Boolean systems has led us to propose the parity expanded network. Much like the state transition graph, it is parity-invariant (up to node relabeling) and completely encodes the system’s dynamics, but its number of nodes grows linearly with the system dimension, rather than exponentially. It unites large knock-out and knock-in (constitutive activity) perturbations within the same framework, greatly simplifying their analysis compared to the similar ideas presented in [31], upon which we build. This earlier construction made use of three types of nodes and lacked explicit dynamical structure, requiring careful case-splitting and multiple system representations to study system perturbations (see e.g., [56]). Rather than distinguish nodes that correspond to on and off states at a definitional level, we distinguish these nodes by their behavior under a global parity transformation. This view elucidates the role of the expanded network as a parity invariant and of its stable motifs as strongly connected components that have no parity-invariant subgraphs. These insights have enabled our formal proofs of novel results that relate network reduction methods, driver sets, and stable motifs -- results which we have leveraged to develop a fast attractor-finding method.

We have presented for the first time the time reversal of a stochastic update Boolean system and demonstrated its usefulness in analyzing the forward-in-time dynamics. Just as stable motifs of a system describe stable spaces in the dynamics, stable motifs in the time reversal of that system describe unstable spaces. This observation is especially helpful in eliminating states when searching for attractors via direct STG construction, or in reducing the number of relevant initial conditions for study. In addition, it demonstrates an important property: the activity of any stable motif of a system or its time-reversal is constant for any attractor. In this way, time-reversal and parity elucidate the “attractor-conserved” quantities of a system’s dynamics. These attractor-conserved quantities are only conserved within attractors and may initially vary. Nonetheless, it is surprising to note that in an inherently stochastic system there is a well-defined notion of time-reversal that yields asymptotic conservation laws.

By combining new results stemming from the parity view of the expanded network with our novel time-reversal construction, we developed a method for fast attractor identification in stochastic update Boolean systems. We employed this new method to explore the scaling in attractor number for asynchronous $N - K$ Kauffman networks. Using these methods, we probed the power law scaling of the $K = 2$ critical ($p = 0.5$) Boolean networks under asynchronous update. Our new techniques allowed us to find or bound the number of attractors in these networks for sizes larger than ever before considered ($N = 16,384$), and indeed we cover much of the biologically relevant ranges of gene regulatory network sizes. The power law scaling we observe is much lower (by a factor of about 10) than the theoretical maximum of $\ln 4$ [72], and also lower than the originally conjectured 0.5 scaling exponent [24].

The low average number of attractors we find ($\langle A \rangle \approx 4$ for networks with $N \approx 4,000$) is consistent with previous results on the average number of point attractors and stable synchronous attractors in this ensemble [59,63].

The relatively slow growth of the average number of attractors compared to (i) the originally conjectured 0.5 scaling exponent and (ii) the current cell type scaling estimate of 0.70 ($0.88/1.26 = 0.70$, based on the experimental data from [44]) has several possible explanations that suggest follow-up investigations. One possibility is that timing-specific attractors contribute significantly to the cell-type scaling, implying that gene-regulatory synchrony plays a crucial role in a cell's ability to differentiate. Alternatively, the scaling of the attractor number under stochastic update might vary between critical RBN ensembles (e.g. it may differ in ensembles using canalizing functions or threshold functions), and some of these other ensembles could more accurately reproduce the observed cell type scaling. Analysis of the attractor number scaling in other RBN ensembles using our approach should help answer this question. It is also possible that gene regulatory networks of living organisms have evolved to increase the number of robust attractors, a process which is not fully captured by these ensembles of RBN.

The methods developed here can be readily applied to the numerous published Boolean models of biological systems to elucidate their full attractor repertoire. Our framework can also bring further insight into a variety of models that could be reformulated as Boolean models. For example, the quenched Glauber dynamics set on a network [80], models of binary opinion propagation [8], or the Hopfield model [23] can be expressed with threshold Boolean functions. The stable motifs of these systems, and correspondingly the trap spaces of their dynamics, can be identified as particular instances of strongly connected subgraphs. Indeed, in the Watts model of opinion propagation the percolation of an opinion depends on the existence of a strongly connected subgraph of early adopters, who can be influenced by a single neighbor to adopt the opinion [18]. We expect that future adaptation of our methods to these models will be able to reveal rare attractors (metastable states).

Apart from the direct application to Boolean models we have emphasized here, time reversal and parity play a role in describing the fundamental logical relationships between entities in complex systems more generally. In this view, the logical parity inversion and time reversal of a system describe a coarse-grained and discretized version of the dynamics, which in turn provides insight into the dynamics of more detailed models (see e.g. [46,81] for further discussion). While the extent to which our key results generalize beyond the stochastic Boolean systems presented here remains an open question, we are encouraged by preexisting analogs of expanded networks in multi-level systems [57] and ODEs [58], as well as by results connecting logic-based models to ODEs [46,81–83]. Though our focus here is at the level of interaction logic, our results suggest a new approach to analyzing complexity: studying the relationship of a complex system to its logical parity inversion and time reversal to constrain the system's repertoire of emergent behaviors.

Acknowledgements

This work was supported by NSF grants PHY 1545832, MCB 1715826, IIS 1814405 to R.A. and the Stand Up to Cancer Foundation/The V Foundation Convergence Scholar Award to J.G.T.Z. (D2015-039).

References

1. Boccara N. *Modeling Complex Systems*. Springer Science & Business Media; 2010.
2. Schweitzer F. *Brownian Agents and Active Particles: Collective Dynamics in the Natural and Social Sciences*. Springer Science & Business Media; 2007.

3. Shalizi CR. Methods and Techniques of Complex Systems Science: An Overview. *Topics in Biomedical Engineering International Book Series*. 2006. pp. 33–114. doi:10.1007/978-0-387-33532-2_2
4. Sayama H. Introduction to the Modeling and Analysis of Complex Systems. Open SUNY Textbooks; 2015.
5. Vespignani A. Modelling dynamical processes in complex socio-technical systems. *Nature Physics*. 2012. pp. 32–39. doi:10.1038/nphys2160
6. Mora T, Bialek W. Are biological systems poised at criticality? *J Stat Phys*. 2011;144: 268–302.
7. Ramaswamy S. The Mechanics and Statistics of Active Matter. 2010 [cited 6 Jul 2020]. doi:10.1146/annurev-conmatphys-070909-104101
8. Castellano C, Fortunato S, Loreto V. Statistical physics of social dynamics. *Reviews of Modern Physics*. 2009. pp. 591–646. doi:10.1103/revmodphys.81.591
9. Motter AE, Timme M. Antagonistic Phenomena in Network Dynamics. *Annu Rev Condens Matter Phys*. 2018;9: 463–484.
10. Strogatz SH. Nonlinear Dynamics and Chaos. 2018. doi:10.1201/9780429492563
11. Tyson JJ, Novak B. A Dynamical Paradigm for Molecular Cell Biology. *Trends Cell Biol*. 2020;30: 504–515.
12. Railsback SF, Grimm V. Agent-Based and Individual-Based Modeling: A Practical Introduction, Second Edition. Princeton University Press; 2019.
13. Toffoli T, Margolus N. Cellular Automata Machines: A New Environment for Modeling. MIT Press; 1987.
14. Barabási A-L. Network Science. Cambridge University Press; 2016.
15. Newman M. Networks. 2010. doi:10.1093/acprof:oso/9780199206650.001.0001
16. Li F, Long T, Lu Y, Ouyang Q, Tang C. The yeast cell-cycle network is robustly designed. *Proc Natl Acad Sci U S A*. 2004;101: 4781–4786.
17. Espinosa-Soto C, Padilla-Longoria P, Alvarez-Buylla ER. A gene regulatory network model for cell-fate determination during *Arabidopsis thaliana* flower development that is robust and recovers experimental gene expression profiles. *Plant Cell*. 2004;16: 2923–2939.
18. Watts DJ. A simple model of global cascades on random networks. *The Structure and Dynamics of Networks*. 2011. doi:10.1515/9781400841356.497
19. Vollmer H. Introduction to Circuit Complexity. *Texts in Theoretical Computer Science An EATCS Series*. 1999. doi:10.1007/978-3-662-03927-4
20. Glauber RJ. Time-Dependent Statistics of the Ising Model. *J Math Phys*. 1963;4: 294–307.
21. Godrèche C, Luck JM. Metastability in zero-temperature dynamics: statistics of attractors. *Journal of Physics: Condensed Matter*. 2005. pp. S2573–S2590. doi:10.1088/0953-8984/17/24/014
22. McCulloch WS, Pitts W. A logical calculus of the ideas immanent in nervous activity. *The Bulletin of Mathematical Biophysics*. 1943. pp. 115–133. doi:10.1007/bf02478259
23. Hopfield JJ. Neural networks and physical systems with emergent collective computational abilities. *Proceedings of the National Academy of Sciences*. 1982. pp. 2554–2558. doi:10.1073/pnas.79.8.2554
24. Kauffman SA. Metabolic stability and epigenesis in randomly constructed genetic nets. *J Theor Biol*. 1969;22: 437–467.
25. Thomas R. Boolean formalization of genetic control circuits. *J Theor Biol*. 1973;42: 563–585.
26. Samaga R, Klamt S. Modeling approaches for qualitative and semi-quantitative analysis of cellular signaling networks. *Cell Communication and Signaling*. 2013. p. 43. doi:10.1186/1478-811x-11-43
27. Kim J, Park S-M, Cho K-H. Discovery of a kernel for controlling biomolecular regulatory networks. *Scientific Reports*. 2013. doi:10.1038/srep02223
28. Mendoza L. A network model for the control of the differentiation process in Th cells. *Biosystems*. 2006. pp. 101–114. doi:10.1016/j.biosystems.2005.10.004
29. Naldi A, Carneiro J, Chaouiya C, Thieffry D. Diversity and Plasticity of Th Cell Types Predicted from Regulatory Network Modelling. *PLoS Computational Biology*. 2010. p. e1000912.

doi:10.1371/journal.pcbi.1000912

- 30. Sánchez L, Thieffry D. A Logical Analysis of the Drosophila Gap-gene System. *Journal of Theoretical Biology*. 2001. pp. 115–141. doi:10.1006/jtbi.2001.2335
- 31. Albert R, Othmer HG. The topology of the regulatory interactions predicts the expression pattern of the segment polarity genes in *Drosophila melanogaster*. *J Theor Biol*. 2003;223: 1–18.
- 32. Cohen DPA, Martignetti L, Robine S, Barillot E, Zinovyev A, Calzone L. Mathematical Modelling of Molecular Pathways Enabling Tumour Cell Invasion and Migration. *PLOS Computational Biology*. 2015. p. e1004571. doi:10.1371/journal.pcbi.1004571
- 33. Steinway SN, Zanudo JGT, Ding W, Rountree CB, Feith DJ, Loughran TP, et al. Network Modeling of TGF Signaling in Hepatocellular Carcinoma Epithelial-to-Mesenchymal Transition Reveals Joint Sonic Hedgehog and Wnt Pathway Activation. *Cancer Research*. 2014. pp. 5963–5977. doi:10.1158/0008-5472.can-14-0225
- 34. Udyavar AR, Wooten DJ, Hoeksema M, Bansal M, Califano A, Estrada L, et al. Novel Hybrid Phenotype Revealed in Small Cell Lung Cancer by a Transcription Factor Network Model That Can Explain Tumor Heterogeneity. *Cancer Res*. 2017;77: 1063–1074.
- 35. Eduati F, Jaaks P, Wappler J, Cramer T, Merten CA, Garnett MJ, et al. Patient-specific logic models of signaling pathways from screenings on cancer biopsies to prioritize personalized combination therapies. *Molecular Systems Biology*. 2020. doi:10.1525/msb.20188664
- 36. Zañudo JGT, Mao P, Alcon C, Kowalski KJ, Johnson GN, Xu G, et al. Cell-line-specific network models of ER+ breast cancer identify PI3K α inhibitor sensitivity factors and drug combinations. 2020. p. 2020.08.25.261370. doi:10.1101/2020.08.25.261370
- 37. Albert R, Acharya BR, Jeon BW, Zañudo JGT, Zhu M, Osman K, et al. A new discrete dynamic model of ABA-induced stomatal closure predicts key feedback loops. *PLoS Biol*. 2017;15: e2003451.
- 38. Ohta N, Waki K, Mochizuki A, Satou Y. A Boolean Function for Neural Induction Reveals a Critical Role of Direct Intercellular Interactions in Patterning the Ectoderm of the Ascidian Embryo. *PLoS Comput Biol*. 2015;11: e1004687.
- 39. Sahin O, Fröhlich H, Löbke C, Korf U, Burmester S, Majety M, et al. Modeling ERBB receptor-regulated G1/S transition to find novel targets for de novo trastuzumab resistance. *BMC Syst Biol*. 2009;3: 1.
- 40. Bonzanni N, Garg A, Feenstra KA, Schütte J, Kinston S, Miranda-Saavedra D, et al. Hard-wired heterogeneity in blood stem cells revealed using a dynamic regulatory network model. *Bioinformatics*. 2013;29: i80–8.
- 41. Rodríguez-Jorge O, Kempis-Calánis LA, Abou-Jaoudé W, Gutiérrez-Reyna DY, Hernandez C, Ramirez-Pliego O, et al. Cooperation between T cell receptor and Toll-like receptor 5 signaling for CD4 T cell activation. *Sci Signal*. 2019;12. doi:10.1126/scisignal.aar3641
- 42. Aldana M, Coppersmith S, Kadanoff LP. Boolean Dynamics with Random Couplings. *Perspectives and Problems in Nonlinear Science*. 2003. pp. 23–89. doi:10.1007/978-0-387-21789-5_2
- 43. Drossel B. Random Boolean Networks. *Reviews of Nonlinear Dynamics and Complexity*. 2008. pp. 69–110. doi:10.1002/9783527626359.ch3
- 44. Bornholdt S, Kauffman S. Ensembles, dynamics, and cell types: Revisiting the statistical mechanics perspective on cellular regulation. *J Theor Biol*. 2019;467: 15–22.
- 45. Abou-Jaoudé W, Traynard P, Monteiro PT, Saez-Rodriguez J, Helikar T, Thieffry D, et al. Logical Modeling and Dynamical Analysis of Cellular Networks. *Frontiers in Genetics*. 2016. doi:10.3389/fgene.2016.00094
- 46. Thomas R. On the Relation Between the Logical Structure of Systems and Their Ability to Generate Multiple Steady States or Sustained Oscillations. *Springer Series in Synergetics*. 1981. pp. 180–193. doi:10.1007/978-3-642-81703-8_24
- 47. Richard A. Positive and negative cycles in Boolean networks. *J Theor Biol*. 2019;463: 67–76.
- 48. Klarner H, Bockmayr A, Siebert H. Computing maximal and minimal trap spaces of Boolean networks. *Natural Computing*. 2015. pp. 535–544. doi:10.1007/s11047-015-9520-7

49. Wang R-S, Albert R. Elementary signaling modes predict the essentiality of signal transduction network components. *BMC Systems Biology*. 2011. doi:10.1186/1752-0509-5-44
50. Zañudo JGT, Albert R. An effective network reduction approach to find the dynamical repertoire of discrete dynamic networks. *Chaos: An Interdisciplinary Journal of Nonlinear Science*. 2013. p. 025111. doi:10.1063/1.4809777
51. Klarner H, Streck A, Siebert H. PyBoolNet: a python package for the generation, analysis and visualization of boolean networks. *Bioinformatics*. 2016. p. btw682. doi:10.1093/bioinformatics/btw682
52. Deritei D, Rozum J, Regan ER, Albert R. A feedback loop of conditionally stable circuits drives the cell cycle from checkpoint to checkpoint. *Scientific Reports*. 2019. doi:10.1038/s41598-019-52725-1
53. Zañudo JGT, Albert R. Cell Fate Reprogramming by Control of Intracellular Network Dynamics. *PLOS Computational Biology*. 2015. p. e1004193. doi:10.1371/journal.pcbi.1004193
54. Steinway SN, Zañudo JGT, Michel PJ, Feith DJ, Loughran TP, Albert R. Combinatorial interventions inhibit TGF β -driven epithelial-to-mesenchymal transition and support hybrid cellular phenotypes. *NPJ Syst Biol Appl*. 2015;1: 15014.
55. Maheshwari P, Albert R. A framework to find the logic backbone of a biological network. *BMC Systems Biology*. 2017. doi:10.1186/s12918-017-0482-5
56. Yang G, Zañudo JGT, Albert R. Target Control in Logical Models Using the Domain of Influence of Nodes. *Frontiers in Physiology*. 2018. doi:10.3389/fphys.2018.00454
57. Gan X, Albert R. General method to find the attractors of discrete dynamic models of biological systems. *Physical Review E*. 2018. doi:10.1103/physreve.97.042308
58. Rozum JC, Albert R. Identifying (un)controllable dynamical behavior in complex networks. *PLOS Computational Biology*. 2018. p. e1006630. doi:10.1371/journal.pcbi.1006630
59. Klemm K, Bornholdt S. Stable and unstable attractors in Boolean networks. *Phys Rev E Stat Nonlin Soft Matter Phys*. 2005;72: 055101.
60. Zheng D, Yang G, Li X, Wang Z, Liu F, He L. An Efficient Algorithm for Computing Attractors of Synchronous And Asynchronous Boolean Networks. *PLoS ONE*. 2013. p. e60593. doi:10.1371/journal.pone.0060593
61. Garg A, Mohanram K, Di Cara A, De Micheli G, Xenarios I. Modeling stochasticity and robustness in gene regulatory networks. *Bioinformatics*. 2009;25: i101–9.
62. Wuensche A. *Exploring Discrete Dynamics*. Luniver Press; 2011.
63. Bossomaier T., Harvey I. Time out of joint: Attractors in Asynchronous Random Networks. *Proceedings of the Fourth European Conference on Artificial Life*. MIT Press; pp. 67–75.
64. Zhang R, Shah MV, Yang J, Nyland SB, Liu X, Yun JK, et al. Network model of survival signaling in large granular lymphocyte leukemia. *Proceedings of the National Academy of Sciences*. 2008. pp. 16308–16313. doi:10.1073/pnas.0806447105
65. Saadatpour A, Wang R-S, Liao A, Liu X, Loughran TP, Albert I, et al. Dynamical and structural analysis of a T cell survival network identifies novel candidate therapeutic targets for large granular lymphocyte leukemia. *PLoS Comput Biol*. 2011;7: e1002267.
66. Naldi A, Remy E, Thieffry D, Chaouiya C. Dynamically consistent reduction of logical regulatory graphs. *Theoretical Computer Science*. 2011. pp. 2207–2218. doi:10.1016/j.tcs.2010.10.021
67. Veliz-Cuba A. Reduction of Boolean network models. *J Theor Biol*. 2011;289: 167–172.
68. Deritei D, Aird WC, Ercsey-Ravasz M, Regan ER. Principles of dynamical modularity in biological regulatory networks. *Scientific Reports*. 2016. doi:10.1038/srep21957
69. Derrida B, Pomeau Y. Random Networks of Automata: A Simple Annealed Approximation. *EPL*. 1986;1: 45.
70. Socolar JES, Kauffman SA. Scaling in Ordered and Critical Random Boolean Networks. *Physical Review Letters*. 2003. doi:10.1103/physrevlett.90.068702
71. Villani M, Campioli D, Damiani C, Roli A, Filisetti A, Serra R. Dynamical regimes in non-ergodic random Boolean networks. *Natural Computing*. 2017. pp. 353–363. doi:10.1007/s11007-016-

72. Greil F, Drossel B. Dynamics of critical Kauffman networks under asynchronous stochastic update. *Phys Rev Lett.* 2005;95: 048701.

73. Gershenson C. Updating Schemes in Random Boolean Networks. *Artificial Life IX.* 2004. doi:10.7551/mitpress/1429.003.0040

74. Trinh VG, Hiraishi K. A Study on Attractors of Generalized Asynchronous Random Boolean Networks. *IEICE Transactions on Fundamentals of Electronics, Communications and Computer Sciences.* 2020. pp. 987–994. doi:10.1587/transfun.2019eap1163

75. Lambert SA, Jolma A, Campitelli LF, Das PK, Yin Y, Albu M, et al. The Human Transcription Factors. *Cell.* 2018. pp. 650–665. doi:10.1016/j.cell.2018.01.029

76. Dufresne A, Salanoubat M, Partensky F, Artiguenave F, Axmann IM, Barbe V, et al. Genome sequence of the cyanobacterium Prochlorococcus marinus SS120, a nearly minimal oxyphototrophic genome. *Proceedings of the National Academy of Sciences.* 2003. pp. 10020–10025. doi:10.1073/pnas.1733211100

77. Blattner FR. The Complete Genome Sequence of Escherichia coli K-12. *Science.* 1997. pp. 1453–1462. doi:10.1126/science.277.5331.1453

78. Consortium THGS, The Honeybee Genome Sequencing Consortium. Insights into social insects from the genome of the honeybee *Apis mellifera*. *Nature.* 2006. pp. 931–949. doi:10.1038/nature05260

79. Venter JC et al. The Sequence of the Human Genome. *Science.* 2001. pp. 1155.4–1155. doi:10.1126/science.291.5507.1155d

80. Castellano C, Loreto V, Barrat A, Cecconi F, Parisi D. Comparison of voter and Glauber ordering dynamics on networks. *Phys Rev E Stat Nonlin Soft Matter Phys.* 2005;71: 066107.

81. Rozum JC, Albert R. CONTROLLING THE CELL CYCLE RESTRICTION SWITCH ACROSS THE INFORMATION GRADIENT. *Advances in Complex Systems.* 2019. p. 1950020. doi:10.1142/s0219525919500206

82. Krumsiek J, Pölsterl S, Wittmann DM, Theis FJ. Odefy -- From discrete to continuous models. *BMC Bioinformatics.* 2010. p. 233. doi:10.1186/1471-2105-11-233

83. Rozum JC, Albert R. Self-sustaining positive feedback loops in discrete and continuous systems. *Journal of Theoretical Biology.* 2018. pp. 36–44. doi:10.1016/j.jtbi.2018.09.017

Supplementary Materials

Text S1: Background on Random Boolean Networks

The Kauffman $N - K$ random Boolean network (RBN) model [1] has been frequently studied in systems biology and statistical physics for over 50 years. In this model, each of N nodes receives K edges from randomly selected nodes, and the (quenched) update functions are chosen such that each of 2^K input combinations yields an output of 1 with probability p . These models traditionally use the *synchronous update* scheme, in which all variables are updated simultaneously at each time-step, making the system's dynamics deterministic. Their attractors exhibit many features of biological cells, including stability against random external perturbations and plausible scaling laws for the number of attractors and attractor cycle lengths with the number of nodes N [2,3]. Specifically, tuning the indegree K or the activation bias p can produce an order-to-chaos transition at $2Kp(1 - p) = 1$ (in the thermodynamic limit, when $N \rightarrow \infty$) [4,5]. In the ordered regime, almost all nodes quickly attain a stationary state and small, transient perturbations tend to dissipate. In the chaotic regime, on the other hand, the number of fluctuating nodes is proportional to N and perturbations grow exponentially fast. At $2Kp(1 - p) = 1$ there is a so-called critical regime in which, on average, small perturbations persist indefinitely but remain small. RBNs with more heterogeneous topologies [6] or alternative distributions of update functions [7–11] also exhibit these regimes. The networks of greatest interest for biological systems were conjectured to lie near the critical regime [2]. More recent work analyzing the dynamical behavior of gene regulatory networks [12–15] and studying evolutionary models of gene regulatory networks [16,17] has provided further support for this conjecture.

There has been a rich history of research on the scaling of the average number of attractors with network size in the biologically relevant critical regime (see [3] for a review of this work). Based on the relationship between the number of cell types and DNA content, Kauffman originally conjectured that the average number of attractors grows with the number of genes as a power law with exponent $1/2$ [1,2]. In the half-century since the introduction of the $N - K$ ensemble, numerical and theoretical analyses by multiple research groups have shown that the scaling of the number of attractors depends on the updating scheme and is not necessarily a power law [18–24]. Under synchronous update, the average number of attractors for the $K = 2, p = 0.5$ critical Kauffman networks grows faster than any power law (in contrast to earlier conjectures) [23]. Many of these attractors rely on perfect synchrony of multiple nodes. However, the assumption of synchronicity is not suitable for systems that exhibit multiple time scales or stochasticity [25,26]. In contrast, under stochastic asynchronous update, the number of attractors grows as a power law, with an upper bound given by $N^{\ln 4} \approx N^{1.39}$ [20]. The existence of a power law scaling in the asynchronous case is supported by a study of stable synchronous attractors (which are preserved under a perturbation of node update synchrony) in networks of up to $N = 40$ nodes [25]. This study reported an exponent of 0.5 and a low average number of stable synchronous attractors (1.6 for $N = 30$). Another relevant result is that in $N - K$ ensembles with $p = 0.5$ the average number of point attractors is 1, regardless of the value of N or K (implying that for large N at least a small number of nodes oscillate in most attractors) [27]. Importantly, for the $K = 2$ critical Kauffman networks under stochastic asynchronous update, the exact value of the power law exponent is still unknown.

Text S2: Formal definitions of auxiliary networks

The expanded network is a hypergraph constructed from a Boolean system's update rules and is defined as follows. Each node I of the expanded network, called a *virtual node*, is an ordered pair $I = (n(I), s(I))$ consisting of a system entity, in this context denoted $n(I)$, and a value $s(I)$, which is either the constant 1 or the constant 0. In a Boolean

model there are two virtual nodes associated with each system entity i , namely $(i, 1)$ and $(i, 0)$; we call this pair of virtual nodes *contradictory*. A set of virtual nodes that does not contain any contradictory pair is called *consistent*. The activity variable for I , written σ_I , is the Boolean literal $X_{n(I)}$ if $s(I) = 1$ or $\neg X_{n(I)}$ if $s(I) = 0$ (σ_I can be written agnostically as $\neg X_{n(I)} \text{ xor } s(I)$). The value of σ_I in a state X is written $\sigma_I(X)$. For example, if we consider a virtual node $I = (i, 0)$, then $\sigma_I(X) = 1$ holds when X_i is 0 in state X . A set of virtual nodes S is *active* (in a system state X) if all its members are active (i.e., if $\sigma_I(X) = 1$ for all $I \in S$). The update function F_I for each virtual node's activity is inherited from the update function for $n(I)$, i.e., $F_{(i,1)}(X) = f_i(X)$ and $F_{(i,0)}(X) = \neg f_i(X)$ are the update functions for $(i, 1)$ and $(i, 0)$; note that the activity of contradictory virtual nodes must always be updated together and have opposite states. A *hyperedge* connects a set of parent virtual nodes $S = \{I_0, I_1, \dots, I_k\}$ to a target virtual node J if $\Lambda_{I \in S} \sigma_I$ is a prime implicant of F_J .

The *succession diagram*, Σ , of a Boolean system is a directed acyclic graph whose nodes are the unions of stable motifs. Considering two nodes P and Q of the succession diagram Σ , there is an edge from P to Q if there is a stable motif M of the reduction $Red(f, P)$ of f by P such that $Q = P \cup M$. For example, in Figure 3 of the main text the reduction by the blue stable motif (panel D) contains the pink stable motif, thus the succession diagram (panel E) contains an edge from the blue stable motif to the union of the blue and pink stable motifs. Each path in the succession diagram $p = (p_0 = \{\}, p_1, \dots, p_n = P)$ from the empty set to a node $P \in \Sigma$ defines a stable motif history $M_i = p_{i+1} \setminus p_i$ for $i = 0..n - 1$ and a corresponding sequence of reduced systems $Red(f, p_i)$. For each sink node of the succession diagram (i.e., whenever a reduced system has no additional stable motifs) there is guaranteed to be an attractor in which all reduced variables are fixed in their reduced states. If any variables remain unreduced, then one or more of the unreduced variables oscillate in the attractor. By repeating the reduction for every possible choice of stable motifs, one can construct a list of attractors of the Boolean system. For an example of this process, see Figure 3 of the main text.

Text S3: Formal statements and proofs of key results

Theorem 1 and its corollaries relate an attractor to the domains of influence of driver sets that activate in said attractor.

Theorem 1: If an attractor \mathcal{A} contains a state X in which the set of virtual nodes S is active, then \mathcal{A} contains a state for which $DOI(S) \cup S$ is active.

Proof of Theorem 1: By definition, \mathcal{A} contains all system states reachable from X by all (stochastic asynchronous) update orders. In particular, it contains the set \mathcal{A}' of all states reachable by update orders in which the variables described by S are never updated and remain fixed at their values in X . Consider the modified system obtained by replacing the update functions f_i for X_i by the constant function $f_i(X) = s$ for all $(i, s) \in S$. By definition, the set $DOI(S)$ consists of all virtual nodes $(j, u) \notin S$ for which $X_j = u$ is fixed in all attractors of the modified system. It may also contain elements of S , but this is irrelevant when considering \mathcal{A}' because S is active in all states in \mathcal{A}' by definition. In particular, $DOI(S) \cup S$ is active in all attractor states of the modified system. Because S is active in both the modified system and along the paths from X to the states in \mathcal{A}' , it follows that all paths that start from X in the modified system can reach \mathcal{A}' . Therefore, \mathcal{A}' contains an attractor of the modified system and thus a state for which $DOI(S) \cup S$ is active.

Two corollaries of Theorem 1 require us to introduce the concept of *contradiction boundary*. If a virtual node I is not consistent with a set of virtual nodes S , but there is a path from a subset of S to I with all path nodes except I consistent with S , then we say that I is in the *contradiction boundary* of S . In this case the LDOI of S will contain a parent node of I , but it will not contain I . If S is internally inconsistent (i.e., if it contains contradictory virtual nodes), then we say that the contradiction boundary of S is the set of contradictory virtual node pairs in S . The contradiction

boundary captures whether a set of virtual nodes S will eventually activate a state that contradicts S . If the contradiction boundary of S is non-empty, we say that S is *self-negating*. The concept of contradiction boundary is important because of the following property: if S is self-negating, then there is no attractor of the system in which all of S is permanently active.

Corollary 1: If $DOI(i, s)$ contains a stable module (or motif), M , then in every attractor either 1) M is active, or 2) X_i is fixed in state $\neg s$ (or both).

Proof of Corollary 1: If 2) does not hold in an attractor \mathcal{A} , then \mathcal{A} contains a state X in which $S = \{(i, s)\}$ is active. Thus, by Theorem 1, \mathcal{A} contains a state in which $DOI(i, s)$, and M in particular, activates. The permanency of the activation of stable modules (and motifs) implies that if M is active in any state of \mathcal{A} , it is active in all states of \mathcal{A} . Therefore, 1) and 2) cannot both fail to be true.

Corollary 2: Let Δ be a set of single-node drivers of a collection of mutually consistent stable modules (or motifs). If there exists an attractor \mathcal{A} in which none of these stable modules (or motifs) are active, then $\neg\Delta$ is not self-negating (its contradiction boundary is empty).

Corollary 2 follows immediately from Corollary 1, as discussed in the main text.

Lemma 1 and Theorem 2 formalize the relationship between deletion projection of [28, 29] and stable motif analysis.

Lemma 1: Let f_i be the update functions of a stochastic asynchronous Boolean system and f_i^{red} be a deletion projection of f_i with projection map π . Let X_{red} be any state of the reduced system and S be the set of virtual nodes in the expanded network of f_i that are (1) also in the expanded network of f_i^{red} , and (2) active in X_{red} . Then S has the property that $DOI(S) \cup S$ is active in exactly one state X of the unreduced system.

Proof of Lemma 1: The entire set of virtual nodes $DOI(S) \cup S$ is active in the attractors of the modified system in which S is kept always active (this follows from the definition of domain of influence). Insofar as we consider only transitions that do not involve updates of the nodes constrained by S , the dynamics are unchanged by modifications of the update rules of these variables. In particular, consider the modified system constructed in the proof of Theorem 1 by replacing the update rules f_i for X_i by the constant function $f_i(X) = s$ for all $(i, s) \in S$. The deletion projection procedure does not depend on the form of these modified update functions because their corresponding variables are not deleted; thus in this modified system, the deletion project takes the form $f_i^{red}(X) = s$. Then, following the convention that constant variables are removed, the deletion projection completely reduces the system to the 0-dimensional system, via the projection map that sends every X_i to s . The point attractor correspondence demonstrated in (Naldi et al. 2011) then implies that the original system also has exactly one attractor and that it is a point attractor satisfying $X_i = s$ for all $(i, s) \in S$. Because the point attractor specifies a value for every node, it follows that $DOI(S) \cup S$ is active in exactly one state.

This lemma is closely related to various results in [91] regarding what are therein called “representative states”. Lemma 1 tells us that fixing the state of the variables specified by S (which is given by the state of all variables of the projected system) will result in a steady state in the unprojected system. It leads to a key result about the relationship between the deletion projection method and stable motifs: the activity of stable motifs in attractors of the projected system is indicative of their activity in attractors of the original system and vice versa. Theorem 2 makes this correspondence precise.

Theorem 2: Let f_i be the update functions of a stochastic asynchronous Boolean system that has a stable module (or motif) M and an attractor \mathcal{A} . Further, let f_i^{red} be a deletion projection of f_i with projection map π . Let \mathcal{A}_{red} be an arbitrary attractor of the deletion projection with $\mathcal{A}_{red} \subseteq \pi(\mathcal{A})$. The following implications hold:

1. If M is active in \mathcal{A} then each state of \mathcal{A}_{red} can be lifted to a state with M active (i.e., M is active in some state of $\pi^{-1}(X_{red})$ for every state $X_{red} \in \mathcal{A}_{red}$) and
2. If any state X_{red} in \mathcal{A}_{red} can be lifted to a state with M active (i.e., if M is active in some element of $\pi^{-1}(X_{red})$), then M is active in \mathcal{A} .

Proof of Theorem 2: First, note that \mathcal{A}_{red} exists by Theorem 1, part 3 in [28]. Next, the two parts of the theorem are proved separately.

1. Assume M is active in \mathcal{A} . Consider any state $X_{red} \in \mathcal{A}_{red}$. Because $\mathcal{A}_{red} \subseteq \pi(\mathcal{A})$, there exists $X \in \mathcal{A}$ such that $\pi(X) = X_{red}$. Because M is active in \mathcal{A} , it is in particular active in X . Therefore, X is a state in $\pi^{-1}(X_{red})$ in which M is active.
2. Assume \mathcal{A}_{red} contains a state X_{red} such that M is active in some state $X \in \pi^{-1}(X_{red})$. Consider the set S of $\dim f_i^{red}$ virtual nodes in the expanded network of f_i that are active in all states that map to X_{red} under π . By Lemma 1, $DOI(S) \cup S$ is active in exactly one state. Because M and S are both active in X and M describes a trap space, it follows that $DOI(S) \cup S$ cannot contradict M . Because $DOI(S) \cup S$ is active in only one state, this implies that M is active in $DOI(S) \cup S$. Then from $X_{red} \in \mathcal{A}_{red} \subseteq \pi(\mathcal{A})$, it follows that \mathcal{A} contains at least one state in $\pi^{-1}(X_{red})$, and thus it contains a state in which S is active. Thus, by Thm. 1, \mathcal{A} contains a state in which $DOI(S) \cup S$, and M in particular, is active. Because M describes a trap space, its activation is irreversible. Therefore, M is active in all of \mathcal{A} .

Text S4: Identifying terminal reduced networks using time reversal and drivers

In general, testing for terminality requires analysis of the system's state transition graph. This approach, however, is computationally expensive; the STG can have as many as $2^N N$ edges (i.e., for $f_i(X) = \neg X_i$, $i = 1..N$). To avoid excess computation in special cases in which terminality can be determined without state-space simulation, we conduct a series of simple tests using necessary or sufficient conditions for terminality for every reduced system $G = Red(f, P)$ with $P \in \Sigma$.

The first and simplest of these tests is to examine the out-degree of P . If P has out-degree zero in the succession diagram Σ , then G does not contain stable motifs and is trivially terminal. A second test is supplied by Corollary 2 (see Text S3). We consider the set Δ of all virtual nodes that individually drive any stable motif of G . By Corollary 2, all members of Δ must be inactive in any motif-avoidant attractor. For example, in Figure 4, the virtual node (C,1) is a driver of the stable motif marked in green, so X_C must be inactive in any motif-avoidant attractor. To identify any attractors of G in which all of Δ is inactive, we consider the negated set $\neg\Delta$ and its logical domain of influence, $LDOI(\neg\Delta)$. If G is terminal, then it has an attractor in which these sets are both active. Furthermore, if $\neg\Delta$ is stably active in some attractor, then the update values of the variables constrained by $\neg\Delta$ must also be fixed in the corresponding states. For example, in Figure 4, because $X_C = 0$ must hold for all states in any motif-avoidant attractor, f_C must also be zero in that attractor. We summarize these various non-terminality conditions by the algebraic constraint that all motif-avoidant attractor states of G satisfy $R(X) = 1$, where $R(X) = \bigwedge_{I \in \neg\Delta} (\sigma_I(X) \wedge F_I(X)) \wedge (\bigwedge_{J \in LDOI(\neg\Delta)} \neg\sigma_J(X))$. In the example of Figure 4, there is only one single-node driver of the system's sole stable motif, namely (C,1). Thus, the entire negated driver set is $\neg\Delta = \{(C, 0)\}$. We calculate that $LDOI(C, 0)$ is empty and that the update function for (C,0) is $F_{(C,0)} = \neg X_A \vee \neg X_B$. Therefore, we find $R(X) = \neg X_C \wedge (\neg X_A \vee \neg X_B)$. In panel C

of Figure 4, only the three yellow states have $R(X) = 1$, and so any motif- avoidant attractor is confined to those three states

Text S5: Simulation and further reduction of the relevant state space

If we are unable to rule out the possibility that the reduced system G is terminal, we conduct a state-space search for attractors that do not activate any stable motifs in G . Because we are only concerned with a subset of the state-space, we are able to avoid simulating some of the states for an increase in computational speed. We achieve this by keeping track of a set of system states in the state transition graph of G , $STG(G)$, that cannot be part of any motif-avoidant attractor. We denote this set of system states K . Initially, K is the terminal restriction space of G . We take each state of the state transition graph that is not in K , i.e. each state $X \in V(STG(G)) \setminus K$ and compute its successors using the Boolean update rules. If X has a successor in K , then X and all its ancestor states in $STG(G)$ (i.e., all states from which we have previously found a path to X) are added to K . Similarly, X and its ancestors are added to K if there is a stable motif M^- of $TR(G)$ active in X , but inactive in one of its successors. The subgraph $STG(G) \setminus K$ of $STG(G)$ necessarily contains any attractors that are in G but none of its network reductions. These attractors are identified as the terminal strongly connected components in $STG(G) \setminus K$.

There are two major computational benefits to this approach to simulating a reduced STG. First, each stable motif of a reduced system G constrains at least one variable, so the size of the state space is reduced by at least a factor of two for every stable motif in G . Second, for a given STG, the task of finding attractors is equivalent to the task of finding terminal strongly connected components, which scales linearly with the number of edges in the STG [30]. As such, reducing the size of the directed graph that must be searched for attractors generally results in drastically improved performance. The degree to which performance is increased depends upon the final size of the set K , which itself depends on the stable motif structure of G and of its time reversal.

In cases for which other simulation methods are computationally prohibitive, we resort to the deletion projection method and application of Theorem 2 in order to investigate terminality of a motif-reduced Boolean system. We find the attractors of the projected system and test whether each projection attractor is inconsistent (in the sense of Theorem 2) with all stable motifs. If none of the projection attractors are inconsistent, then the reduced system from which the projection was constructed is necessarily not terminal. Otherwise, the deletion reduction has motif-avoidant attractors. If the motif-reduced system has a motif-avoidant attractor, it necessarily corresponds to one or more of the motif-avoidant attractors of the deletion projection. In this way, the number of motif-avoidant attractors of the deletion projection places an upper bound on the number of motif-avoidant attractors of the motif-reduced system.

Text S6: Analysis of a T-LGL model using time-reversal

To illustrate the new insights that the expanded network framework and the time-reversal system can bring, we analyze a simplified network model [31] of a type of white blood cell cancer (T-LGL leukemia) shown in Figure S6.1. This model considers the relationships between five proteins (denoted “cer”, “disc”, “fas”, “flip”, and “s1p”) and the process of cell death (apoptosis, denoted “apo”). The governing update functions are as follows:

$$\begin{aligned}
 f_{apo}(X) &= X_{disc} \vee X_{apo} \\
 f_{cer}(X) &= \neg X_{apo} \wedge X_{fas} \wedge \neg X_{s1p} \\
 f_{disc}(X) &= (\neg X_{apo} \wedge X_{fas} \wedge \neg X_{flip}) \vee (\neg X_{apo} \wedge X_{cer}) \\
 f_{fas}(X) &= \neg X_{apo} \wedge \neg X_{s1p} \\
 f_{flip}(X) &= \neg X_{apo} \wedge \neg X_{disc}
 \end{aligned}$$

$$f_{s1p}(X) = \neg X_{apo} \wedge \neg X_{cer}$$

Previous analysis of the model indicated that it has two attractors, one corresponding to a T-LGL (cancerous) state and one corresponding to the normal behaviour (apoptosis). We find that the system has three stable motifs, indicated in Figure S6.1A. Two of these are mutually consistent and describe trap spaces that contain the cancerous state, while the third contains the apoptotic state. The time-reversed system contains two stable motifs (Figure S6.1B), which together partition the state space into four regions (Figure S6.1C). The virtual node sets that define two of these regions (R1 and R2) are self-negating, meaning that these regions cannot contain attractors. The stable motif $\{(apo,1)\}$ is active in all states of region R4. The LDOI of this stable motif specifies that fixing $apo=1$ drives the rest of the variables into their inactive states (see the edges originating from the blue virtual node in Figure S6.1A). Thus, region R4 contains the point attractor corresponding to apoptosis, which is the larger bold-outlined dark-blue node in Figure S6.1E. The stable motifs colored in red in Figure S6.1A are active in the subset of region R3 that corresponds to irreversible commitment to the T-LGL point attractor. The flow between the four regions can be readily determined (see thick dashed arrows in Figure S6.1E). The flow between regions indicates that all system decisions about which attractor to select occur in regions R1 and R3. Any trajectory in R1 may result in the initiation of the apoptosis process ($X_{apo} = 1$) and thus exit R1 via R2, which ultimately leads to the apoptotic attractor. Otherwise, trajectories eventually exit into region R3. In region R3, there are two possibilities: one of the TLG-L stable motifs activates, or the system escapes the region into R4 and the apoptotic attractor. This second scenario is possible because the restriction of the system to R3 (by setting $X_{apo} = 0$) gives rise to a so-called conditional stable motif [32] $\{(cer,1),(fas,1),(s1p,0)\}$, that is self-sustaining in R3, but ultimately drives (disc,1), which in turn drives (apo,1) and exit from R3 into R4, where it is no longer self-sustaining. The four states in which $\{(apo,0),(cer,1),(fas,1),(s1p,0)\}$ is active (colored in light blue in Figure S6.1E) are therefore in the exclusive basin of attraction of the apoptosis attractor (i.e. the set of states from which every trajectory leads to the apoptosis attractor). Thus, by combining the inter-region flow with the irreversibility of stable motifs and the properties of driver sets, we recapitulate the previously obtained exclusive basins of the two attractors (in light blue and dark blue for the apoptosis attractor and in red for the cancerous attractor in Figure S6.1E). In summary, analysis of the expanded network and of the time-reversed system allows an efficient and informative partitioning of the state space and identifies which of the partitions may and which may not contain an attractor.

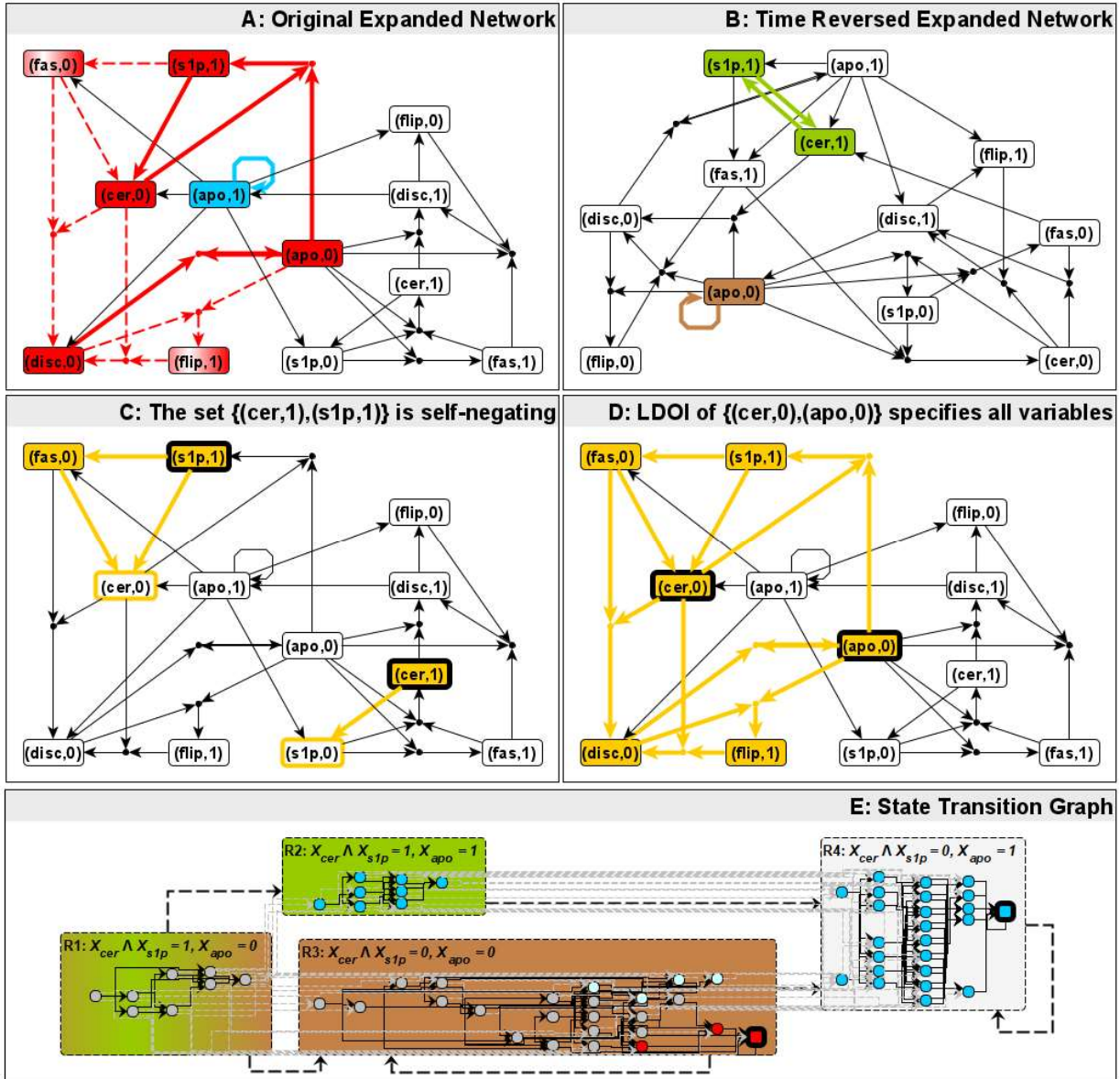


Figure S6.1: Time reversal and domain of influence analysis of the simplified T-LGL leukemia network of [31]. Panel A depicts the expanded network of the system with its stable motifs highlighted in red and blue, respectively (the two partially shaded red nodes and the dotted hyperedges connected to them indicate that a stable motif is formed even when either $(fas,0)$ or $(flip,1)$ is omitted). Panel B depicts the system's time reversal, with its stable motifs highlighted in green and brown, respectively. The stable motifs of the system's time reversal allow us to partition the state-space into four regions according to which time-reversal stable motifs are active: R1) $X_{cer} \wedge X_{s1p} = 1, X_{apo} = 0$, R2) $X_{cer} \wedge X_{s1p} = 1, X_{apo} = 1$, R3) $X_{cer} \wedge X_{s1p} = 0, X_{apo} = 0$, and R4) $X_{cer} \wedge X_{s1p} = 0, X_{apo} = 1$. The properties of Garden of Eden spaces (which include R1, R1UR2, and R1UR3), imply that no attractor lies in more than one of these regions. Any attractor in R1 or R2 has $\{(cer,1),(s1p,1)\}$ active, but this set of virtual nodes is self-negating. The LDOI of this set is depicted in yellow in panel C, with the white nodes with yellow border indicating the nodes that cause the set to be self-negating, i.e., these nodes are the set's contradiction boundary, as defined in Text S3. In any attractor in R3, either $\{(s1p,0),(apo,0)\}$ or $\{(cer,0),(apo,0)\}$ (or both) is active. The first of these is self-negating, but the LDOI of the second of these (depicted in yellow in panel D) fixes all variables, implying that R3 contains a single attractor: the point attractor corresponding to the

highlighted virtual nodes. By a similar argument, R4, defined by the activity of either $\{(s1p,0),(apo,1)\}$ or $\{(cer,0),(apo,1)\}$ contains a single point attractor and no oscillations. The partitioning of the (forward time) STG according to the four regions is depicted in panel E, with each region colored according to which time-reversal stable motifs are active therein. States in the STG are colored in dark blue or red according to whether the stable motifs of the corresponding color are active in each state. The two point attractors are highlighted by bold outlines and are larger than other nodes. For the T-LGL attractor (red), the exclusive basin of attraction coincides with the activation of the corresponding stable motifs. In the apoptosis attractor (blue), the exclusive basin of attraction contains all states in which the apoptosis stable motif is active (dark blue), as well as four additional states (light blue) that can be identified by considering stable motifs of the system obtained by fixing $X_{apo} = 0$ (see text). Grey states may lead to either attractor depending on the stochastic update order. Solid black arrows indicate intra-region state transitions. Dashed arrows indicate inter-region transitions; the light grey arrows connect states in different regions, while the thick dashed lines summarize these state transitions as region to region transitions. A self-loop on a region indicates that it contains an attractor. Notably, the thick dashed lines illustrate the instability property of Garden of Eden spaces: once a trajectory exits the union of R1 and R2, for example, it can never return.

Text S7: Details of the cell cycle Phase Switch model of Deritei et al. (2016)

The model of the cell cycle Phase Switch we consider here is an 11-variable network of interactions among proteins that govern mammalian cells' entry and exit from mitosis (cell division). The model was introduced in [33] and further analyzed in [32]. The update functions are given below; we use the entity name and the name of its corresponding variable interchangeably (e.g., CyclinA should be understood to mean $X_{CyclinA}$ in the functions below).

$f_{Cdc25C} = \text{CyclinA or (CyclinB and Cdk1)}$
 $f_{Cdh1} = \text{not CyclinA and (not CyclinB or not Cdk1)}$
 $f_{Cdk1} = \text{Cdc25C and (CyclinA or CyclinB) and (Cdk1 or not Wee1)}$
 $f_{CyclinA} = (\text{CyclinA or Cdc25A}) \text{ and not (pAPC or Cdh1 and UbcH10)}$
 $f_{CyclinB} = (\text{not pAPC and not Cdh1}) \text{ or (not Cdc20 and not Cdk1)}$
 $f_{pAPC} = (\text{pAPC and Cdc20}) \text{ or (CyclinB and Cdk1)}$
 $f_{Cdc20} = \text{pAPC and not Cdh1 and not Mad2}$
 $f_{UbcH10} = \text{not Cdh1 or (UbcH10 and Cdc20) or (UbcH10 and CyclinA) or (UbcH10 and CyclinB)}$
 $f_{Mad2} = (\text{not pAPC or not Cdc20}) \text{ and CyclinB and Cdk1}$
 $f_{Wee1} = \text{not CyclinA and not CyclinB or not Cdk1}$
 $f_{Cdc25A} = \text{CyclinA and Cdh1}$

This system has three point attractors, which correspond to distinct phases of the cell cycle, namely the G1 (first growth) phase, the G2 (second growth) phase, and the spindle assembly checkpoint (SAC). The G1 attractor is made up by $Cdc25C = Cdk1 = CyclinA = CyclinB = pAPC = Cdc20 = UbcH10 = Mad2 = Cdc25A = 0$, $Cdh1 = Wee1 = 1$. The G2 attractor is made up by $Cdc25C = CyclinA = CyclinB = UbcH10 = Wee1 = Cdc25A = 1$, $Cdk1 = Cdh1 = pAPC = Cdc20 = Mad2 = 0$. The SAC attractor is made up by $Cdc25C = Cdk1 = CyclinB = pAPC = UbcH10 = 1$, $CyclinA = Cdh1 = Cdc20 = Wee1 = Cdc25A = 0$.

The stable motifs of this system and of its reduced networks are labeled as follows

$P0 := \{(CyclinA, 0), (Cdc25A, 0)\}$
 $P1 := \{(Cdk1, 0), (Wee1, 1)\}$
 $P2 := \{(Cdc20, 0), (CyclinB, 1), (Cdc25C, 1), (Cdk1, 1), (Cdh1, 0), (Mad2, 1)\}$
 $P3 := \{(Cdc25, 0), (Cdk1, 0)\}$
 $P4 := \{(CyclinB, 0), (Cdh1, 1)\}$
 $P5 := \{(pAPC, 0)\}$

$P_6 := \{(CyclinA, 1), (Cdh1, 0)\}$

Supplemental Figures S1-S3

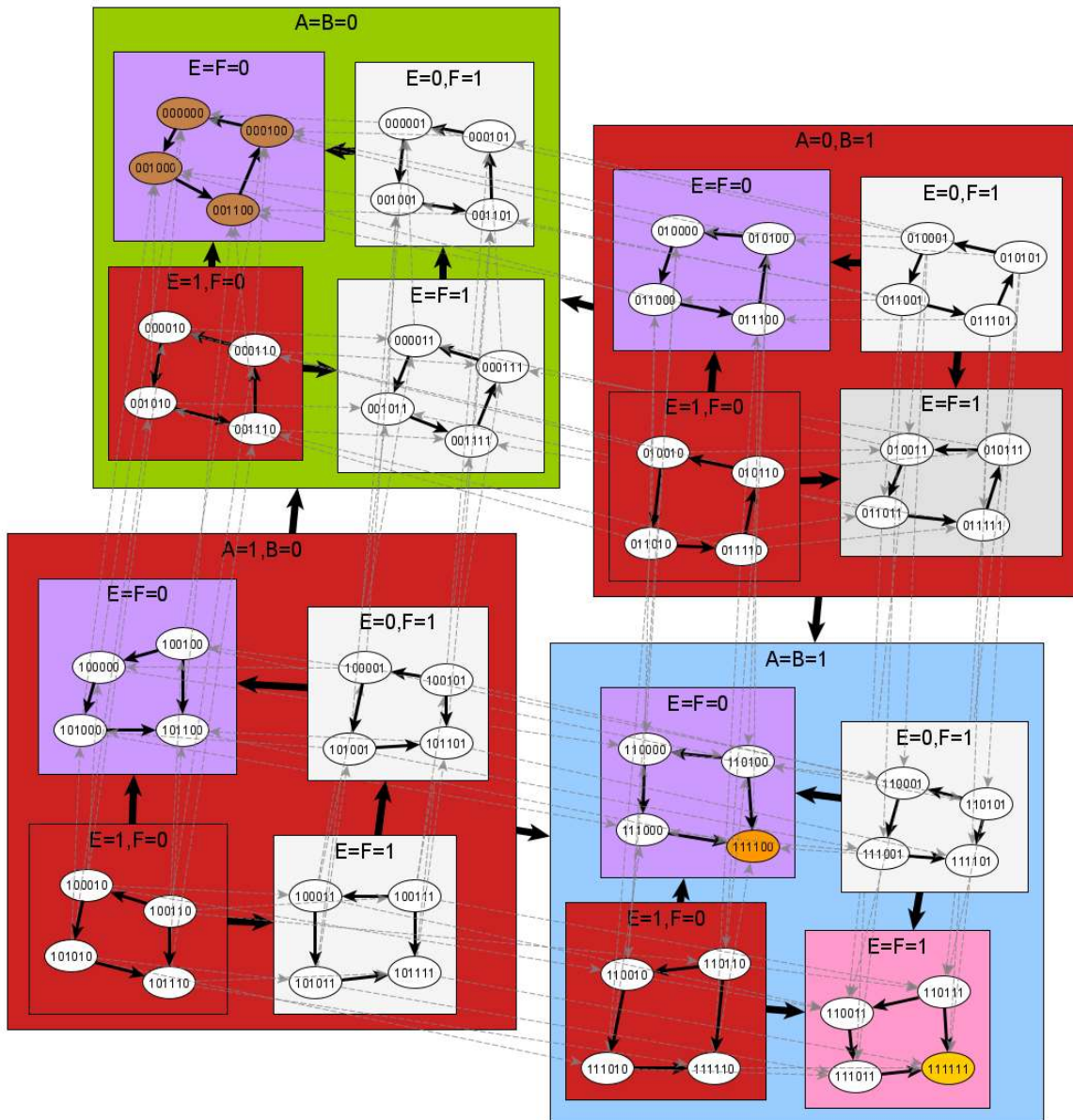


Figure S1: The state transition graph of the example from Figure 3. The state nodes are labeled according to the values of the variable X_A through X_F , in alphabetical order. The states that make up the system's

three attractors are highlighted in yellow, orange, and brown. State transitions are represented by grey dashed arrows, and the transitions between various groupings of nodes, or between nodes within a group, are summarized by solid black arrows. The states are grouped according to the nodes of the succession diagram in Figure 3E, with matching colors (green, purple, pink, and blue). Note that each of these state groups is a trap space in the sense that there are no transitions out of any of the stable motif regions. In addition, three additional groups are highlighted in red: the states in which $X_E = 0$ and $X_F = 1$; the states in which $X_A = 0$ and $X_B = 1$; and the states in which $X_A = 1$ and $X_B = 0$. These three groups are the states in which the time reversed system's three stable motifs are active. As such, these groups are "Garden of Eden" spaces. Indeed, there are no state transitions into any red group from outside that group. The state transition graph indicates that the system irreversibly leaves the Garden-of-Eden spaces and commits to increasingly restricted trap spaces. A particular example of a possible trajectory is to start from a state in the top right group of states (red box with $A=0, B=1$), enter the bottom right group of states (blue box with $A=B=1$), then enter the group of states with pink background ($E=F=1$), then converge into the attractor marked in yellow. This trajectory corresponds to the top branch of the stable motif succession diagram of Figure 3E.

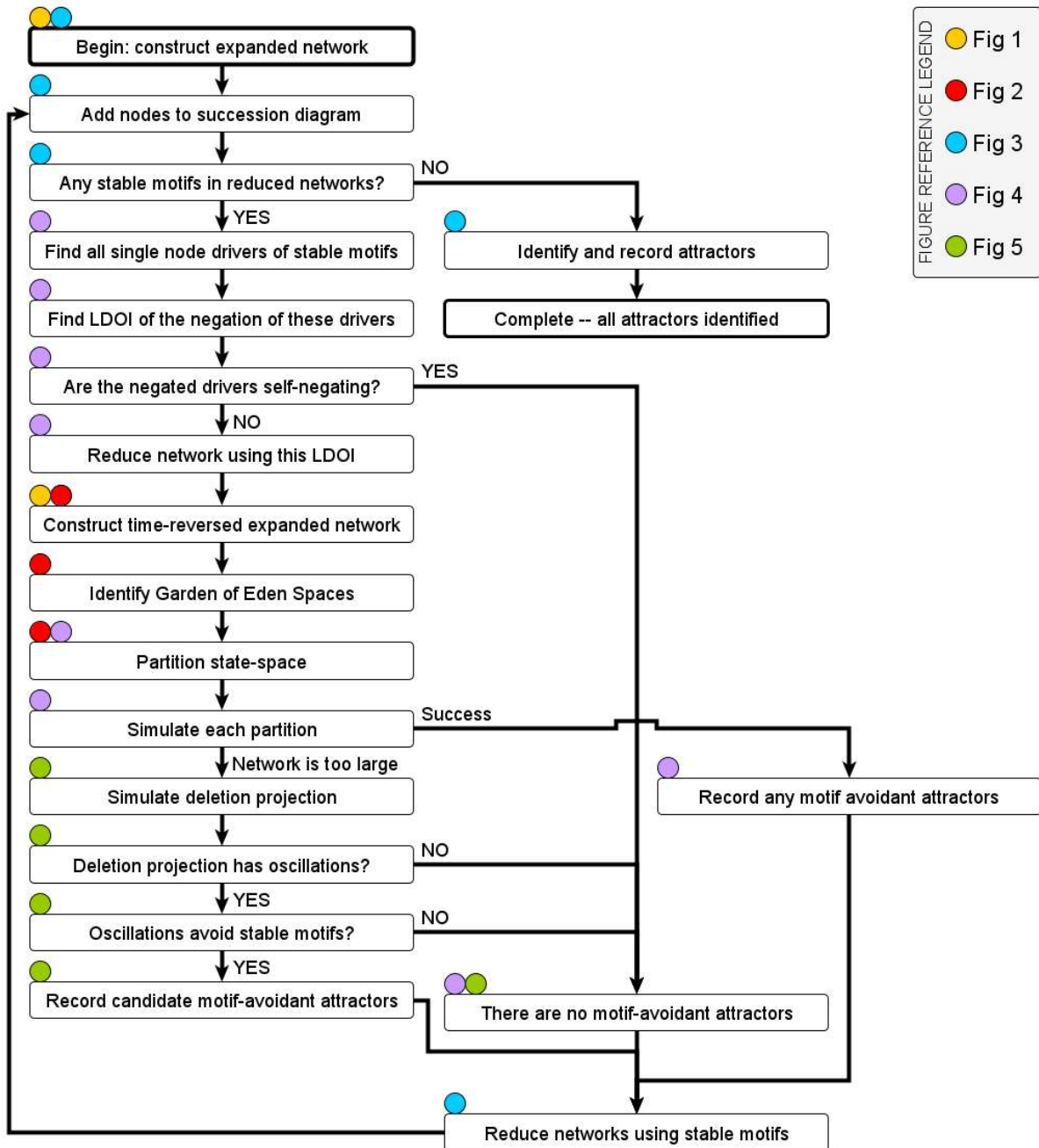


Figure S2: Flowchart illustrating the procedure for generating a succession diagram. Steps are tagged with colored circles indicating which figures provide additional detail for each step. The method for constructing a succession diagram is similar to that presented in Figure 3, but with the additional step of searching for stable motif avoidant attractors using the methods summarized in Figures 4 and 5, which rely on special properties of driver nodes and Boolean time reversal (Figure 2). In brief, the approach is to iteratively consider every possible sequence of stable motif activation (of any length, including zero). The system is simplified under the assumption that all stable motifs in the sequence are active. We then determine whether there are attractors that do not activate any stable motifs of the reduced system. If such an attractor exists, or if the reduced system does not contain stable motifs, the sequence of stable

motifs is called terminal. The set of terminal sequences is in surjective correspondence with the attractors of the system.

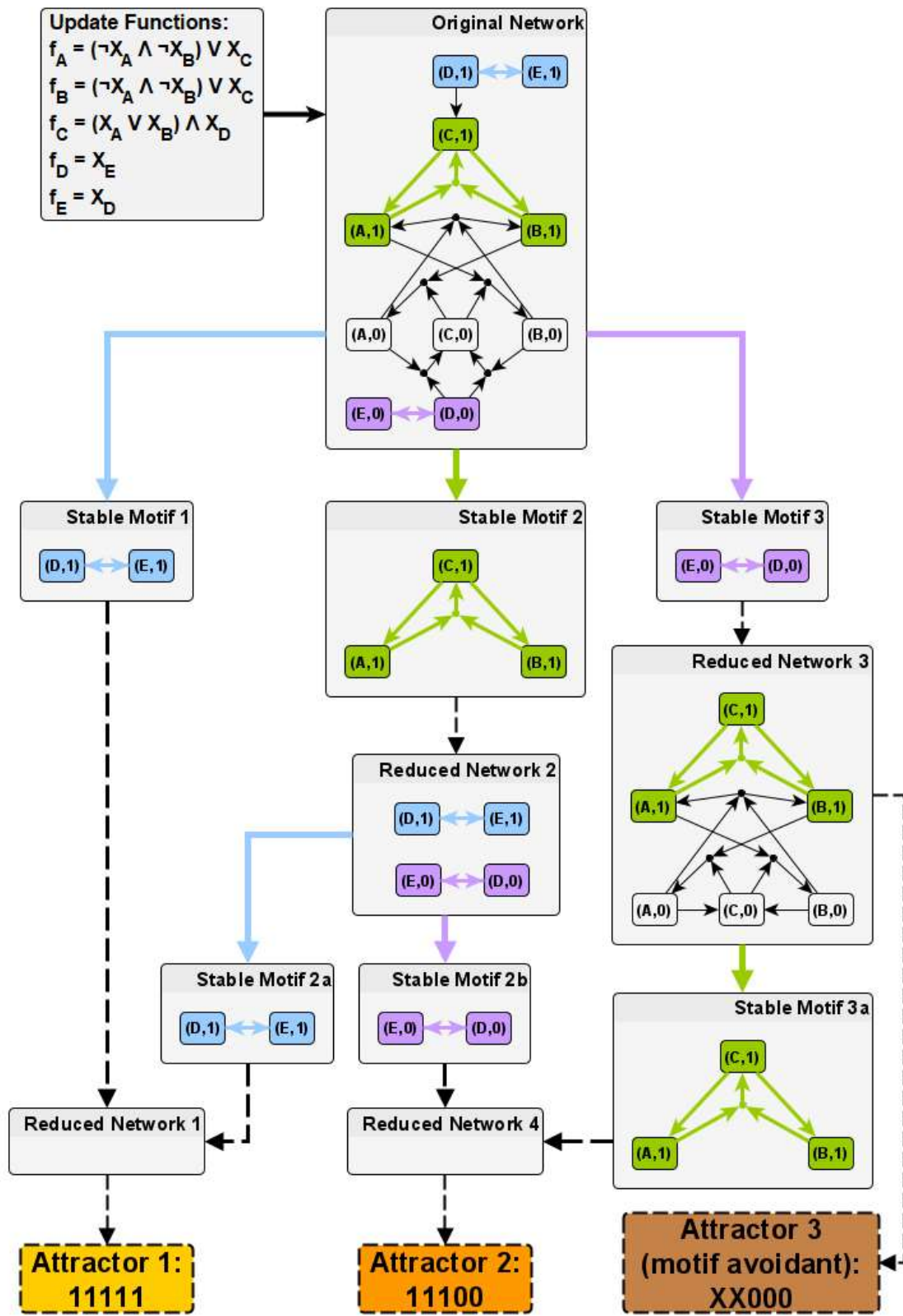


Figure S3: Application of the attractor identification algorithm on a five-variable example with update functions indicated in the top left panel. The expanded network of the system is shown in the topmost center panel (Original Network), and below it are the three stable motifs it contains (labeled Stable Motif 1-3). Two of these arise from the E-D positive feedback loop and are mutually exclusive. Stable Motif 1 (blue) is formed by the virtual nodes $(D, 1)$ and $(E, 1)$, either of which can serve as a driver node of the motif. Stable Motif 3 (purple) is formed by the virtual nodes $(D, 0)$ and $(E, 0)$, either of which can serve as a driver node. Stable Motif 2 (green) is formed by the virtual nodes $(A, 1)$, $(B, 1)$, and $(C, 1)$, the last of which is its driver node. The set of single node drivers is thus $\Delta = \{(D, 1), (E, 1), (D, 0), (E, 0), (C, 1)\}$, and so the negated single driver node set is $\neg\Delta = \{(D, 1), (E, 1), (D, 0), (E, 0), (C, 0)\}$, which is self-negating by virtue of being self-contradictory. Therefore, at least one of the three stable motifs must lock in. After selecting a stable motif, the effects of its activation are depicted below it as a reduced network (labeled Reduced Network 1-3, respectively). This pattern is repeated iteratively until the resulting reduced network contains no further stable motifs, indicating that a minimal trap space has been uncovered. Each minimal trap space is typically small and therefore identifying the attractor(s) it contains is trivial. Attractors are listed along the bottom of the figure, with the binary strings indicating the states of the variables, in alphabetical order, that are fixed in each attractor; an 'X' in this string indicates oscillation. At each stage in the reduction process, one must consider whether there are motif-avoidant attractors that exist in a reduced network but fail to activate any of that network's stable motifs. Following the locking in of Stable Motif 1, the expanded network reduces completely, and an "all-on" point attractor is obtained (Attractor 1); thus there are no motif-avoidant attractors on this branch. If Stable Motif 2 activates in the original network, it yields the bistable switch shown in Reduced Network 2. This reduced network has two stable motifs (2a and 2b), either of which results in a fully reduced network and yields Attractor 1 or Attractor 2, respectively. Reduced Network 2 has negated single driver set $\neg\Delta = \{(D, 1), (E, 1), (D, 0), (E, 0)\}$, and thus has no motif-avoidant attractors (i.e., either Stable Motif 2a or 2b must eventually activate). Finally, if instead Stable Motif 3 locks in, the example of Figure 4 is obtained (Reduced Network 3); this system has one motif-avoidant oscillation (Attractor 3, which involves the oscillation of two of the nodes in such a way that Stable Motif 3a never activates) and one point attractor (Attractor 2) that is reached if the Stable Motif 3a is activated rather than avoided.

Supplementary Code: Jupyter Notebook (Python 3) and input data for attractor scaling fits.

References for Text S1-S7

1. Kauffman SA. Metabolic stability and epigenesis in randomly constructed genetic nets. *J Theor Biol.* 1969;22: 437–467.
2. Kauffman SA. *The Origins of Order: Self Organization and Selection in Evolution*. Oxford University Press, USA; 1993.
3. Bornholdt S, Kauffman S. Ensembles, dynamics, and cell types: Revisiting the statistical mechanics perspective on cellular regulation. *J Theor Biol.* 2019;467: 15–22.
4. Aldana M, Coppersmith S, Kadanoff LP. Boolean Dynamics with Random Couplings. *Perspectives and Problems in Nolinear Science*. 2003. pp. 23–89. doi:10.1007/978-0-387-21789-5_2
5. Derrida B, Pomeau Y. Random Networks of Automata: A Simple Annealed Approximation. *EPL*. 1986;1: 45.
6. Aldana M, Cluzel P. A natural class of robust networks. *Proc Natl Acad Sci U S A*. 2003;100: 8710–8714.
7. Kauffman S, Peterson C, Samuelsson B, Troein C. Genetic networks with canalizing Boolean rules are always stable. *Proc Natl Acad Sci U S A*. 2004;101: 17102–17107.
8. Peixoto TP. The phase diagram of random Boolean networks with nested canalizing functions. *Eur*

Phys J B. 2010;78: 187–192.

- 9. Szejka A, Mihaljev T, Drossel B. The phase diagram of random threshold networks. *New J Phys.* 2008;10: 063009.
- 10. Zañudo JGT, Aldana M, Martínez-Mekler G. Boolean Threshold Networks: Virtues and Limitations for Biological Modeling. *Information Processing and Biological Systems*. Springer, Berlin, Heidelberg; 2011. pp. 113–151.
- 11. Rohlf T, Bornholdt S. Criticality in random threshold networks: annealed approximation and beyond. *Physica A: Statistical Mechanics and its Applications*. 2002. pp. 245–259. doi:10.1016/s0378-4371(02)00798-7
- 12. Nykter M, Price ND, Aldana M, Ramsey SA, Kauffman SA, Hood LE, et al. Gene expression dynamics in the macrophage exhibit criticality. *Proc Natl Acad Sci U S A.* 2008;105: 1897–1900.
- 13. Shmulevich I, Kauffman SA, Aldana M. Eukaryotic cells are dynamically ordered or critical but not chaotic. *Proc Natl Acad Sci U S A.* 2005;102: 13439–13444.
- 14. Balleza E, Alvarez-Buylla ER, Chaos A, Kauffman S, Shmulevich I, Aldana M. Critical dynamics in genetic regulatory networks: examples from four kingdoms. *PLoS One.* 2008;3: e2456.
- 15. Daniels BC, Kim H, Moore D, Zhou S, Smith HB, Karas B, et al. Criticality Distinguishes the Ensemble of Biological Regulatory Networks. *Phys Rev Lett.* 2018;121: 138102.
- 16. Torres-Sosa C, Huang S, Aldana M. Criticality is an emergent property of genetic networks that exhibit evolvability. *PLoS Comput Biol.* 2012;8: e1002669.
- 17. Bornholdt S, Rohlf T. Topological evolution of dynamical networks: global criticality from local dynamics. *Phys Rev Lett.* 2000;84: 6114–6117.
- 18. Bilke S, Sjunnesson F. Stability of the Kauffman model. *Phys Rev E Stat Nonlin Soft Matter Phys.* 2002;65: 016129.
- 19. Soclar JES, Kauffman SA. Scaling in Ordered and Critical Random Boolean Networks. *Physical Review Letters.* 2003. doi:10.1103/physrevlett.90.068702
- 20. Greil F, Drossel B. Dynamics of critical Kauffman networks under asynchronous stochastic update. *Phys Rev Lett.* 2005;95: 048701.
- 21. Flyvbjerg H. An order parameter for networks of automata. *Journal of Physics A: Mathematical and General.* 1988. pp. L955–L960. doi:10.1088/0305-4470/21/19/006
- 22. Bastolla U, Parisi G. The modular structure of Kauffman networks. *Physica D: Nonlinear Phenomena.* 1998. pp. 219–233. doi:10.1016/s0167-2789(97)00242-x
- 23. Kaufman V, Mihaljev T, Drossel B. Scaling in critical random Boolean networks. *Phys Rev E Stat Nonlin Soft Matter Phys.* 2005;72: 046124.
- 24. Villani M, Campioli D, Damiani C, Roli A, Filisetti A, Serra R. Dynamical regimes in non-ergodic random Boolean networks. *Natural Computing.* 2017. pp. 353–363. doi:10.1007/s11047-016-9552-7
- 25. Klemm K, Bornholdt S. Stable and unstable attractors in Boolean networks. *Phys Rev E Stat Nonlin Soft Matter Phys.* 2005;72: 055101.
- 26. Papin JA, Hunter T, Palsson BO, Subramaniam S. Reconstruction of cellular signalling networks and analysis of their properties. *Nat Rev Mol Cell Biol.* 2005;6: 99–111.
- 27. Bossomaier HA. Time out of joint: Attractors in Asynchronous Random Networks. *Proceedings of the Fourth European Conference on Artificial Life.* MIT Press; pp. 67–75.
- 28. Naldi A, Remy E, Thieffry D, Chaouiya C. Dynamically consistent reduction of logical regulatory graphs. *Theoretical Computer Science.* 2011. pp. 2207–2218. doi:10.1016/j.tcs.2010.10.021
- 29. Veliz-Cuba A. Reduction of Boolean network models. *J Theor Biol.* 2011;289: 167–172.
- 30. Tarjan R. Depth-First Search and Linear Graph Algorithms. *SIAM J Comput.* 1972;1: 146–160.
- 31. Saadatpour A, Wang R-S, Liao A, Liu X, Loughran TP, Albert I, et al. Dynamical and structural analysis of a T cell survival network identifies novel candidate therapeutic targets for large granular lymphocyte leukemia. *PLoS Comput Biol.* 2011;7: e1002267.
- 32. Deritei D, Rozum J, Regan ER, Albert R. A feedback loop of conditionally stable circuits drives the cell cycle from checkpoint to checkpoint. *Scientific Reports.* 2019. doi:10.1038/s41598-019-52725-

33. Deritei D, Aird WC, Ercsey-Ravasz M, Regan ER. Principles of dynamical modularity in biological regulatory networks. *Scientific Reports*. 2016. doi:10.1038/srep21957
34. Test, test. test. 2001. doi:10.2172/1023444